2018-12

Theoretical modelling of a new hybrid wave energy converter in regular waves

Zheng, Siming

10.1016/j.renene.2018.05.051
Renewable Energy
Elsevier

Title:

Theoretical modelling of a new hybrid wave energy converter in regular waves

Author names and affiliations:
Siming Zheng
State Key Laboratory of Hydroscience and Engineering, Tsinghua University, Beijing 100084, China
E-mail address: zhengsm@tsinghua.edu.cn

Yongliang Zhang
State Key Laboratory of Hydroscience and Engineering, Tsinghua University, Beijing 100084, China
E-mail address: yongliangzhang@tsinghua.edu.cn

Corresponding author:
Yongliang Zhang
State Key Laboratory of Hydroscience and Engineering, Tsinghua University, Beijing 100084, China
Tel.: + 86 10 62797802
E-mail address: yongliangzhang@tsinghua.edu.cn

Accepted 15 May 2018

https://doi.org/10.1016/j.renene.2018.05.051

Theoretical modelling of a new hybrid wave energy converter in regular waves

Abstract: A novel hybrid wave energy converter (WEC) consisting of a floating oscillating water column (OWC) and several oscillating floats hinged around is proposed. Both water oscillation of the OWC and the wave-induced relative rotation of each float around the OWC are employed to extract wave power. To carry out the hydrodynamic analysis of the hybrid WEC, a theoretical model based on potential flow theory, separation of variables method and eigen-function matching method is presented. Hydrodynamic interaction between the OWC and the floats oscillating independently in surge, sway, heave, roll, pitch and yaw modes is considered. To verify the correctness of the theoretical hydrodynamic model, a specific example is computed and a numerical code based on a boundary element method is also employed as a comparison. The theoretical results are found in good agreement with ones obtained by using different approaches. The theoretical hydrodynamic model is then adopted to evaluate the dynamic response and power absorption of the hybrid WEC in frequency domain. Additionally, the corresponding isolated OWC and hinged floats are computed, respectively, and compared to demonstrate how to interact beneficially between the OWC and the floats in terms of *q*-factor. Effect of the geometry of both the OWC and the floats, and the spacing distance between them on power exploration of the hybrid WEC is investigated. The results reveal that the hybrid WEC holds a wider bandwidth of frequency response with a higher maximum power capture factor compared with those of the isolated OWC and hinged floats.

Keywords: Wave power; Theoretical hydrodynamic model; Oscillating water column; Floats; Power take-off system

1. Introduction

Ocean wave is a kind of renewable resource and it is estimated that the worldwide ocean waves contain power resource as much as 2TW (Thorpe, 1999). Seeking energy from waves not only helps solve the problems of scarcity of electricity and pure water for the people in coastal regions and remote islands (Babarit et al., 2012; Davies, 2005), but also contributes to improving the earth climate and environment. Since 1970s, over one thousand concepts of wave energy conversion have been proposed in Japan, North America and Europe (Clément et al., 2002; Drew et al., 2009). Reviews of wave energy converter (WEC) technologies can be found in Clément et al. (2002), Falnes (2007), Drew et al. (2009), Falcão (2010), López et al. (2013), Lehmann et al. (2017). Among the large number of WECs, oscillating water columns (OWCs) and nodding WECs are two of the main types.

The OWC is mainly composed of a chamber with an opening to the sea below the water surface. Water column inside the chamber oscillates due to wave excitation, and meanwhile the air above the water column in the chamber passes through a turbine to generate electricity. Specific reviews on OWCs can be found in Heath (2012), Falcão and Henriques (2016). Numerical analysis and tank tests have been widely used to study the hydrodynamic performance of OWCs (Sheng et al., 2014; Sheng and Lewis, 2017; He and Huang, 2014; He and Huang, 2017). In numerical studies of an OWC, it involves a crucial aspect for modelling of the free-surface elevation of a "moonpool" suffering from dynamic air pressure inside the OWC chamber. Regarding to this

problem, one may think of the internal water surface as an imaginary, weightless, rigid piston (disk), which is considered as an extremely thin cylinder oscillating up and down (Sheng et al., 2014). Another alternative method is to model the internal water column as a full cylinder of the same length of the water column (Sheng et al., 2014; Penalba et al., 2017a). Although both of the methods have been widely used and have also shown good approximate results for low frequencies when the wavelength is very long compared with the horizontal length of the OWC chamber, these methods do not correctly model the hydrodynamics, because the dynamic air pressure boundary condition for the internal water surface is not exactly satisfied (Evans, 1982; Falnes, 2002). As a comparison, for some specific OWC devices with simple structures such as two-dimensional OWCs with vertical walls and three-dimensional circular cylindrical OWCs, the theoretical solutions based on the surface pressure distribution model are possible and are more correct (Evans and Porter, 1995; Mavrakos and Konispoliatis, 2012). Evans and Porter (1997) investigated the hydrodynamic properties of a vertical thin-walled cylindrical OWC in the open sea analytically. Later, the cases of the vertical cylindrical OWC at the tip of a breakwater, along a straight coast and at a coastal corner were also studied by Martins-rivas and Mei (2009a, 2009b) and Lovas et al. (2010). More recently, Konispoliatis and Mavrakos (2016) developed a theoretical model for dealing with the hydrodynamic analysis of an array of free-floating OWCs and demonstrated that the radiated waves from each OWC were influenced by the spacing distance between the OWCs.

The nodding WEC is a device that possess one or more floats hinged on an offshore structure or coastline, and captures wave power by utilizing the rotation of these floats. One of the most famous nodding WECs is the Salter's Duck, which was proposed by Stephen Salter at the University of Edinburgh (Salter, 1974). An asymmetrical cross section of the float in Salter's Duck was developed to increase the power absorption from incident waves. Experimental study on Salter's Duck in a narrow tank shown that the power absorption efficiency could be more than 90% (Cruz, 2008). Cruz and Salter (2006) investigated the influences of both the position of the axis of rotation and the submergence ratio on power absorption of a modified version of the Salter's Duck by using a commercial boundary element method package. It was shown that the capture width strongly depended on the position of the axis. Recently, Wu et al. (2017) investigated the power extraction by an array of Salter's Ducks using numerical method. It was revealed that the array with Ducks of smaller width performed better in extracting wave power. SDE wave power device, developed by S.D.E. Ltd in Israel, is another nodding WEC, which consists of a flat float hinged on the coastal line. Rotation of the flat float around the hinged point can be used to generate hydraulic pressure, which is then transformed into electricity (Clément et al., 2002). However, SDE WEC suffers the tidal range problem, leading to an efficiency decline with the change of water level. This disadvantage might be overcome by introducing a unique rotating device between the float and the coastal line (Yang, et al., 2017). Wavestar can be seen as another example of nodding WECs, which is composed of a platform and multiple nodding cylindrical vertically axisymmetric floats hinged around (Nambiar et al., 2015). While, the supporting platform is generally required for an offshore nodding WEC, such as Wavestar, constituting an important part of construction cost and system complexity.

For these two kinds of devices as previously reviewed, the OWC wave energy converter has a proven very high reliability and easy maintenance (Heath 2012) whereas the nodding WECs have been proven with high wave energy capture ratios (Cruz, 2008; Serman and Mei, 1980),

converting wave energy efficiently from the high frequency and steep waves. We make full use of the advantages of these two types of devices, and presented a novel hybrid WEC consisting of a floating OWC moored to the sea bed and several oscillating floats hinged around. Apart from capturing power with the turbine of the OWC, a hydraulic power take-off (PTO) system is also installed between each float and the OWC, therefore the wave-induced relative rotation of each float around the hinge on the OWC can also be employed to extract wave power. Due to the physical connection of the oscillating floats on the OWC, no more mooring system or a special supporting platform for these floats is required and this could obviously reduce both structure complexity and construction cost. It is expected that, with an optimized dimension, interaction between the OWC and the multiple floats can obviously increase the power extraction of the hybrid WEC.

Although power take-off of OWC WECs and nodding WECs has been widely studied, to the authors' knowledge, power absorption by a hybrid WEC consisting of both OWC and nodding WECs has never been conducted. The OWC and the multiple floats of the hybrid WEC could possess regular configuration, thus the theoretical method might be applied in carrying out the first step study on wave diffraction and radiation problems of the WEC. Similar theoretical models have been presented by Siddorn and Eatock Taylor (2008) for an array of truncated cylinders, and Konispoliatis and Mavrakos (2016) for multiple floating OWCs, respectively, nevertheless neither of these models can be used to deal with the interaction between OWC and multiple floats. More recently, Göteman (2017) proposed a theoretical model for a truncated float and a truncated cylinder with moonpool rather than an OWC. It means that the hydrodynamic properties due to the oscillating air pressure inside the chamber, which play significant roles in affecting power absorption of OWC, cannot be considered using her model. Additionally, floats were strictly restrained to only move in heave mode (Göteman, 2017). To study the hydrodynamic characteristics of this hybrid WEC, a theoretical hydrodynamic model based on potential flow theory, separation of variables method and eigen-function matching method is presented in this article, which considers hydrodynamic interaction between the OWC and the floats oscillating independently in different modes. As the second step work, we consider a hybrid WEC, in which the OWC chamber is assumed to be stationary. Response and power absorption of the hybrid WEC are calculated based on the parameters obtained from the theoretical hydrodynamic model. Power absorption by the isolated OWC and the isolated hinged floats are also calculated as a comparison. Additionally, effect of spacing distance between the OWC and the floats on the assessment of wave power extraction is studied.

The rest of this paper is organized as follows. The governing equations and boundary conditions for wave diffraction and wave radiation problems are given in Section 2. Expressions and solutions to both diffracted potentials and radiated potentials together with wave excitation volume flux/forces and hydrodynamic coefficients are presented in Section 3. Power absorptions by a hybrid WEC, an isolated OWC and an array of hinged floats are derived in Section 4. Results and discussion are provided in Section 5. Conclusions are summarized in Section 6.

2. Mathematical model for wave diffraction and radiation

Figure 1 gives one typical configuration of the novel hybrid WEC, in which a circular cylindrical floating OWC and several truncated cylindrical floats are involved. Each float is hinged on the OWC by a rigid arm with a hydraulic float PTO installed between the OWC and the rigid arm. There are some mooring lines connecting the bottom of the OWC to anchors on the sea

bed. When waves pass through the hybrid WEC, both the turbine in OWC and the float PTO capture power from waves.

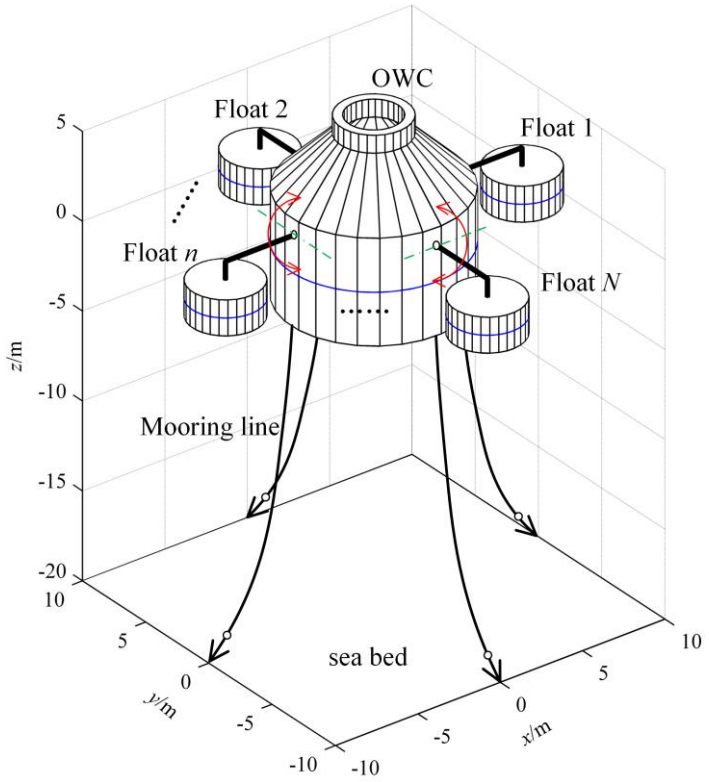

Fig. 1. Sketch of a hybrid WEC under investigation

To study the hydrodynamic characteristics of the hybrid WEC, wave diffraction and wave radiation problems from a cylindrical float with a moonpool (OWC) labelled n=0 and N truncated cylindrical floats labelled n=1,2, …, N moving independently are considered, as shown in Fig. 2. To obtain a more general solution, we assume all the floats with differing radii and draught labelled as R_n and d_n, respectively, in which subscript n denotes Float n, and they are arbitrarily deployed on the free surface of a layer of liquid of finite depth h. Float 0 is used for representing the cylindrical float with a moonpool (OWC). The inner radius of the OWC is denoted as R_i.

A general Cartesian coordinate system $Oxyz$ is adopted with the Oxy plane at the location of the mean water surface, and the Oz axis at the central axis of the OWC pointing upward. Specify the Ox axis arbitrarily, the OWC and truncated floats are subjected to a monochromatic incident wave train of small amplitude A and frequency ω propagating in the direction β relative to the positive Ox axis. Additionally, local cylindrical coordinate systems $Or_n\theta_n$ (n=0, 1, 2, … , N) centered on the origin of the OWC and each float, respectively, are defined, as illustrated in Fig. 2. The rotation center of Float n is (r_n=0, z=z_n) (n=0, 1, 2, …, N), which is used as the reference point to calculate the wave excitation forces and hydrodynamic coefficients in relation with rotary modes. Position of origin of Float n can be written in terms of Cartesian coordinate system $Oxyz$ as (x_n, y_n).

For the purpose of analysis, the fluid is divided as follows (see Fig. 2b): a) fluid domain beneath the OWC and Float n, which are denoted as Region 0 (i.e., $R_i \le r_0 \le R_0$, $-h \le z \le -d_0$) and Region n (i.e., $r_n \le R_n$, $-h \le z \le -d_n$, n=1,2, …, N), respectively; b) fluid domain at the interior region of the OWC and the rest of fluid outside, which are denoted as Region N+1 (i.e., $r_0 \le R_i$, $-h \le z \le 0$)

and Region N+2 (i.e., $r_n \geq R_n$, $-h \leq z \leq 0$), respectively.

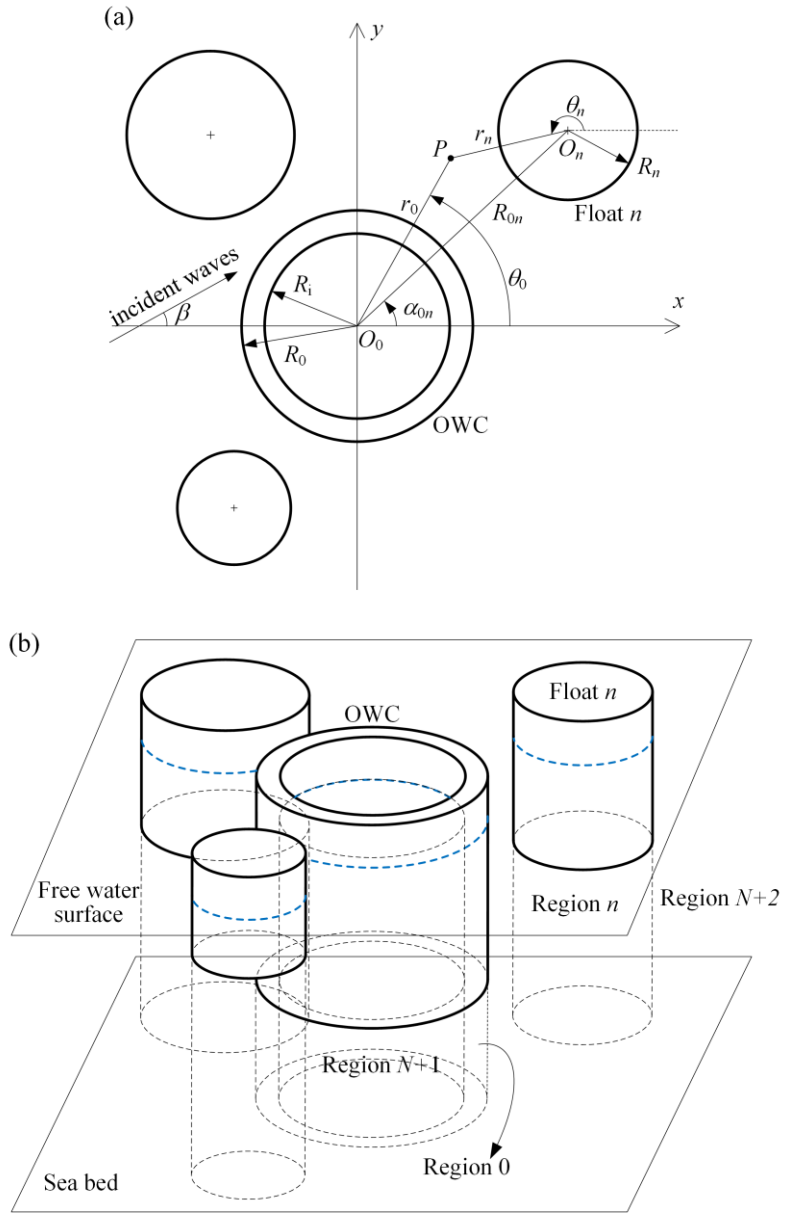

Fig. 2. Definition sketch: a) plan view; b) bird view.

Assuming the fluid to be isotropic and incompressible inviscid, the wave amplitude to be very small, the effect of the turbine in OWC, air compressibility in the chamber and the float PTO to be all linear, linear potential flow theory is adopted. Because of the linearity of the problem, the total spatial velocity potential Φ can be decomposed into the incident wave spatial potential Φ_I, the diffracted wave spatial potential Φ_D and the radiated wave spatial potential as follows

$$\Phi = \Phi_I + \Phi_D + \sum_{n=0}^{N}\sum_{i=1}^{6} \dot{A}_{n,i}\Phi_R^{n,i} + p\Phi_R^{(0)}, \tag{1}$$

where $\dot{A}_{n,i}$ is the velocity complex amplitude of Float n (n=0,1,2,…, N) oscillating in Mode i (i=1~6, which represent surge, sway, heave, roll, pitch, and yaw, respectively); $\Phi_R^{n,i}$ is the spatial

velocity potential due to unit amplitude velocity oscillation of Float n oscillating in Mode i; p is the complex air pressure amplitude inside the OWC chamber; $\Phi_{\mathrm{R}}^{(0)}$ is the spatial velocity potential due to unit air pressure oscillation inside the OWC chamber.

Φ_{I}, Φ_{D}, $\Phi_{\mathrm{R}}^{n,i}$, and $\Phi_{\mathrm{R}}^{(0)}$ all satisfy the Laplace equation and the boundary condition on the impermeable rigid horizontal sea bed. Moreover, Φ_{D}, $\Phi_{\mathrm{R}}^{n,i}$, and $\Phi_{\mathrm{R}}^{(0)}$ must satisfy a radiation condition at infinite distance (Zheng and Zhang, 2015).

Generally, the velocity spatial potential for the undisturbed incident waves with amplitude A and frequency ω propagating in the direction β relative to the positive Ox axis is well known and it can be written as:

$$\Phi_{\mathrm{I}}=-\frac{\mathrm{i}gA}{\omega}\frac{\cosh\left[k\left(z+h\right)\right]}{\cosh\left(kh\right)}\mathrm{e}^{\mathrm{i}k\left(x\cos\beta+y\sin\beta\right)}, \tag{2a}$$

$$\Phi_{\mathrm{I}}\left(r_n,\theta_n,z\right)=-\frac{\mathrm{i}gA}{\omega}\frac{\cosh\left[k\left(z+h\right)\right]}{\cosh\left(kh\right)}\mathrm{e}^{\mathrm{i}k\left(x_n\cos\beta+y_n\sin\beta\right)}\sum_{m=-\infty}^{\infty}\mathrm{i}^m\mathrm{e}^{-\mathrm{i}m\beta}J_m\left(kr_n\right)\mathrm{e}^{\mathrm{i}m\theta_n}, \tag{2b}$$

where Eq.(2a) is written in general Cartesian coordinate system $Oxyz$ and Eq.(2b) is in local cylindrical coordinate systems $Or_n\theta_n$; k is the wave number, which satisfies the dispersion relation $\omega^2=gk\tanh(kh)$; g is the acceleration of gravity; i is the imaginary unit.

The free-surface boundary condition and the body-boundary condition that Φ_{D}, $\Phi_{\mathrm{R}}^{n,i}$, and $\Phi_{\mathrm{R}}^{(0)}$ should satisfy are given as follows:

Wave diffracted potentials:

$$\frac{\partial\Phi_{\mathrm{D}}}{\partial z}-\frac{\omega^2}{g}\Phi_{\mathrm{D}}=0, \quad z=0, \ r_n\geq R_n \ \text{ and } \ r_0<R_{\mathrm{i}} \tag{3}$$

$$\frac{\partial\Phi_{\mathrm{D}}}{\partial z}=-\frac{\partial\Phi_{\mathrm{I}}}{\partial z}, \quad z=-d_n \ \text{ and } \ \delta_{n,0}R_{\mathrm{i}}\leq r_n\leq R_n \tag{4}$$

$$\frac{\partial\Phi_{\mathrm{D}}}{\partial r_n}=-\frac{\partial\Phi_{\mathrm{I}}}{\partial r_n}, \quad -d_n\leq z\leq 0, \ r_n=R_n \ \text{ and } \ r_n=R_{\mathrm{i}} \ \text{ when } n=0 \tag{5}$$

Wave radiated potentials due to the oscillation of Float n (n=0,1,2,3,…N) in Mode i:

$$\frac{\partial\Phi_{\mathrm{R}}^{n,i}}{\partial z}-\frac{\omega^2}{g}\Phi_{\mathrm{R}}^{n,i}=0, \quad z=0, \ r_j\geq R_j \ \text{ and } \ r_0<R_{\mathrm{i}} \tag{6}$$

$$\frac{\partial\Phi_{\mathrm{R}}^{n,i}}{\partial z}=\delta_{n,j}\left(\delta_{3,i}+\delta_{4,i}r_n\sin\theta_n-\delta_{5,i}r_n\cos\theta_n\right), \quad z=-d_j \ \text{ and } \ \delta_{j,0}R_{\mathrm{i}}\leq r_j\leq R_j \tag{7}$$

$$\frac{\partial\Phi_{\mathrm{R}}^{n,i}}{\partial r_j}=\delta_{n,j}\left(\delta_{1,i}\cos\theta_n+\delta_{2,i}\sin\theta_n-\delta_{4,i}\left(z-z_n\right)\sin\theta_n+\delta_{5,i}\left(z-z_n\right)\cos\theta_n\right),$$

$$-d_j\leq z\leq 0, \ r_j=R_j \ \text{ and } \ r_j=R_{\mathrm{i}} \ \text{ when } j=0 \tag{8}$$

Wave radiated potential due to the OWC air pressure oscillation:

$$\frac{\partial \Phi_{\mathrm{R}}^{(0)}}{\partial z}-\frac{\omega^2}{g}\Phi_{\mathrm{R}}^{(0)}=0,\qquad z=0,\ r_j\geq R_j \tag{9a}$$

$$\frac{\partial \Phi_{\mathrm{R}}^{(0)}}{\partial z}-\frac{\omega^2}{g}\Phi_{\mathrm{R}}^{(0)}=\frac{\mathrm{i}\omega}{\rho g},\qquad z=0,\ r_0<R_{\mathrm{i}} \tag{9b}$$

$$\frac{\partial \Phi_{\mathrm{R}}^{(0)}}{\partial z}=0,\qquad z=-d_j \quad \text{and} \quad \delta_{j,0}R_{\mathrm{i}}\leq r_j\leq R_j \tag{10}$$

$$\frac{\partial \Phi_{\mathrm{R}}^{(0)}}{\partial r_j}=0,\qquad -d_j\leq z\leq 0,\ r_j=R_j \quad \text{and} \quad r_j=R_{\mathrm{i}} \quad \text{when } j=0. \tag{11}$$

3 Theoretical solution to diffracted and radiated potentials

3.1 Diffracted/radiated spatial potentials in subdomains

In fluid subdomain Region *j*, the spatial potentials Φ_{D}, $\Phi_{\mathrm{R}}^{n,i}$ (*n*=0, 1, 2, …, *N*), and $\Phi_{\mathrm{R}}^{(0)}$ can be written in a unified format as Φ_j^{χ}, in which χ='D','(*n*,*i*)', and '(0)' represent the corresponding wave diffracted potential, the radiated potential due to the motion of Float *n* in *i*-th mode and the radiated potential due to the air pressure oscillation inside OWC chamber, respectively. In different regions, applying the method of separation, the diffracted/radiated spatial potentials can be expressed by a complex Fourier series as follows:

1) In Region *j* (*j*=0, 1, 2, 3, …, *N*)

$$\Phi_j^{\chi}\left(r_j,\theta_j,z\right)=\Phi_{j,\mathrm{p}}^{\chi}+\sum_{m=-\infty}^{\infty}\left[\frac{D_{m,0}^{\chi,j}}{2}+\sum_{l=1}^{\infty}\left(A_{m,l}^{\chi,j}\frac{I_m\left(\beta_{j,l}r_j\right)}{I_m\left(\beta_{j,l}R_j\right)}+C_{m,l}^{\chi,j}\frac{K_m\left(\beta_{j,l}r_j\right)}{K_m\left(\beta_{j,l}R_j\right)}\right)\cos\left[\beta_{j,l}\left(z+h\right)\right]\right]\mathrm{e}^{\mathrm{i}m\theta_j} \tag{12}$$

where

$$D_{m,0}^{\chi,j}=\begin{cases}A_{m,0}^{\chi,j}+C_{m,0}^{\chi,j}\left[1+\ln\left(\dfrac{r_j}{R_j}\right)\right], & m=0\\ A_{m,0}^{\chi,j}\left(\dfrac{r_j}{R_j}\right)^{|m|}+C_{m,0}^{\chi,j}\left(\dfrac{r_j}{R_j}\right)^{-|m|}, & m\neq 0\end{cases} \tag{13}$$

I_m is the modified Bessel function of first kind and order *m*; K_m is the modified Bessel function of second kind and order *m*; $A_{m,l}^{\chi,j}$ and $C_{m,l}^{\chi,j}$ are unknown coefficients to be solved in Section 3.2, in which $C_{m,l}^{\chi,j}$ vanishes for *j*>0, i.e., the regions beneath of the floats; $\beta_{j,l}$ is the *l*-th eigenvalue in Region *j* (*j*=0, 1, 2, …, *N*) which is given by

$$\beta_{j,l}=\frac{l\pi}{h-d_j},\quad l=0,\ 1,\ 2,\ 3,\ldots \tag{14}$$

$\Phi_{j,\mathrm{p}}^{\chi}$ is a particular solution, which for χ='D', $\Phi_{j,\mathrm{p}}^{\chi}$ =- Φ_{I} ; for χ='(0)', $\Phi_{j,\mathrm{p}}^{\chi}$ vanishes; for χ='(n,i)', $\Phi_{j,\mathrm{p}}^{\chi}$ can be expressed in coordinate system of Float j as

$$\Phi_{\mathrm{R},j,\mathrm{p}}^{(n,i)}=\begin{cases}0, & i=1,2,6\\ \dfrac{\delta_{n,j}}{4\left(h-d_j\right)}\left[2\left(z+h\right)^2-r_j^2\right], & i=3\\ \dfrac{\delta_{n,j}\sin\theta_j}{8\left(h-d_j\right)}\left[4r_j\left(z+h\right)^2-r_j^3\right], & i=4\\ \dfrac{\delta_{n,j}\cos\theta_j}{8\left(h-d_j\right)}\left[r_j^3-4r_j\left(z+h\right)^2\right], & i=5\end{cases} \tag{15}$$

2) Region N+1

$$\Phi_{N+1}^{\chi}\left(r_0,\theta_0,z\right)=\sum_{m=-\infty}^{\infty}\left[\frac{D_{m,0}^{\chi,N+1}J_m\left(kr_0\right)Z_0\left(z\right)}{J_m\left(kR_{\mathrm{i}}\right)Z_0\left(0\right)}+\sum_{l=1}^{\infty}\frac{D_{m,l}^{\chi,N+1}I_m\left(k_lr_0\right)Z_l\left(z\right)}{I_m\left(k_lR_{\mathrm{i}}\right)Z_l\left(0\right)}\right]\mathrm{e}^{\mathrm{i}m\theta_0}+\Phi_{N+1,\mathrm{p}}^{\chi} \tag{16}$$

where $D_{m,l}^{\chi,N+1}$ is the coefficient to be solved in Section 3.2; J_m is the Bessel function of order m; k_l is the eigenvalue which is given by (Falnes, 2002)

$$\omega^2=-k_lg\tan\left(k_lh\right),\qquad l=1,2,3,\ldots \tag{17}$$

$$Z_0\left(z\right)=N_0^{-0.5}\cosh\left[k\left(z+h\right)\right];\quad Z_l\left(z\right)=N_l^{-0.5}\cos\left[k_l\left(z+h\right)\right]; \tag{18}$$

$$N_0=\frac{1}{2}\left[1+\frac{\sinh\left(2kh\right)}{2kh}\right];\quad N_l=\frac{1}{2}\left[1+\frac{\sin\left(2k_lh\right)}{2k_lh}\right]; \tag{19}$$

$\Phi_{N+1,\mathrm{p}}^{\chi}$ is a particular solution, which for χ='(0)', $\Phi_{N+1,\mathrm{p}}^{\chi}=-\mathrm{i}/\left(\rho\omega\right)$; whereas for χ='D' and '(n,i)', $\Phi_{N+1,\mathrm{p}}^{\chi}$ vanishes.

3) Region N+2

The diffracted/radiated spatial potential in Region N+2, can be decomposed into the summation of N+1 cylindrical spatial potentials at the exterior domain as follows:

$$\Phi_{N+2}^{\chi}=\sum_{j=0}^{N}\Phi_j^{\chi,\mathrm{e}}\,. \tag{20}$$

Diffracted spatial potential $\Phi_j^{\chi,\mathrm{e}}$ represents the wave travelling outwards from Float j and can be written in terms of following well-known eigen-function expansion in its own coordinate system:

$$\Phi_j^{\chi,\mathrm{e}}\left(r_j,\theta_j,z\right)=\sum_{m=-\infty}^{\infty}\left[B_{m,0}^{\chi,j}\frac{H_m\left(kr_j\right)}{H_m\left(kR_j\right)}\frac{Z_0\left(z\right)}{Z_0\left(0\right)}+\sum_{l=1}^{\infty}B_{m,l}^{\chi,j}\frac{K_m\left(k_lr_j\right)}{K_m\left(k_lR_j\right)}\frac{Z_l\left(z\right)}{Z_l\left(0\right)}\right]\mathrm{e}^{\mathrm{i}m\theta_j}\,, \tag{21}$$

where H_m is the Hankel function of first kind of order m; $B_{m,l}^{\chi,n}$ are unknown coefficients to be solved in Section 3.2;

Graf's addition theorem for Bessel functions (Abramowitz and Stegun, 1964) is adopted here, thus Φ_{N+2}^{χ} can be expressed in the polar coordinates $O_jr_j\theta_jz$ as (Zheng and Zhang, 2015):

$$\begin{aligned}&\Phi_{N+2}^{\chi}\left(r_j,\theta_j,z\right)\\&=\sum_{m=-\infty}^{\infty}\left[B_{m,0}^{\chi,j}\frac{H_m\left(kr_j\right)}{H_m\left(kR_j\right)}\frac{Z_0\left(z\right)}{Z_0\left(0\right)}+\sum_{l=1}^{\infty}B_{m,l}^{\chi,j}\frac{K_m\left(k_lr_j\right)}{K_m\left(k_lR_j\right)}\frac{Z_l\left(z\right)}{Z_l\left(0\right)}\right]\mathrm{e}^{\mathrm{i}m\theta_j}\\&+\sum_{\substack{j'=0\\j'\neq j}}^{N}\sum_{m=-\infty}^{\infty}\left\{\frac{B_{m,0}^{\chi,j'}}{H_m\left(kR_j\right)}\frac{Z_0\left(z\right)}{Z_0\left(0\right)}\sum_{m'=-\infty}^{\infty}\left(-1\right)^{m'}H_{m-m'}\left(kR_{jj'}\right)J_{m'}\left(kr_j\right)\mathrm{e}^{\mathrm{i}\left(m\alpha_{jj}-m'\alpha_{jj'}\right)}\mathrm{e}^{\mathrm{i}m'\theta_j}\,,\ r_{j'}<R_{jj'}\right.\\&\left.+\sum_{l=1}^{\infty}\frac{B_{m,l}^{\chi,j'}}{K_m\left(k_lR_{j'}\right)}\frac{Z_l\left(z\right)}{Z_l\left(0\right)}\sum_{m'=-\infty}^{\infty}K_{m-m'}\left(k_lR_{jj'}\right)I_{m'}\left(k_lr_j\right)\mathrm{e}^{\mathrm{i}\left(m\alpha_{jj}-m'\alpha_{jj'}\right)}\mathrm{e}^{\mathrm{i}m'\theta_j}\right\}\end{aligned} \tag{22}$$

3.2 Method of computation for unknown coefficients

Expressions of the diffracted and radiated spatial potentials as given in Eqs. (12)~(22) in Sections 3.1 satisfy all the boundary conditions as shown in Eqs. (3) ~ (11) given in Section 2, except those on the interfaces of each two adjacent subdomains r_n=R_n and r_0=R_i. The conditions of continuity for pressure and normal velocity at r_n=R_n and r_0=R_i can be used to determine the unknown coefficients in Eqs. (12)~(22) for both diffracted and radiated spatial potentials.

The continuity conditions for the spatial potentials are given as follows:

1）Continuity of pressure at the boundary r_j=R_j (j=0, 1, 2, …N):

$$\Phi_{N+2}^{\chi}\left(r_j,\theta_j,z\right)=\Phi_j^{\chi}\left(r_j,\theta_j,z\right),\qquad -h<z<-d_j,r_j=R_j\,. \tag{23}$$

2）Continuity of pressure at the boundary r_0=R_i:

$$\Phi_{N+1}^{\chi}\left(r_0,\theta_0,z\right)=\Phi_0^{\chi}\left(r_0,\theta_0,z\right),\qquad -h<z<-d_0,r_0=R_i\,. \tag{24}$$

3）Continuity of normal velocity at the boundary r_j=R_j (j=0, 1, 2, …N):

For $-h<z<-d_j$,

$$\frac{\partial\Phi_{N+2}^{\chi}\left(r_j,\theta_j,z\right)}{\partial r_j}=\frac{\partial\Phi_j^{\chi}\left(r_j,\theta_j,z\right)}{\partial r_j}\,. \tag{25a}$$

For $-d_j<z<0$,

$$\frac{\partial \Phi_{N+2}^{\chi}\left(r_j,\theta_j,z\right)}{\partial r_j}=\begin{cases}-\dfrac{\partial \Phi_{\mathrm{I}}\left(r_j,\theta_j,z\right)}{\partial r_j}, & \chi=\text{'}(0)\text{'}\\ \delta_{n,j}\left[\delta_{1,i}\cos\theta_n+\delta_{2,i}\sin\theta_n\right. & \\ \quad\left.-\delta_{4,i}\left(z-z_n\right)\sin\theta_n+\delta_{5,i}\left(z-z_n\right)\cos\theta_n\right], & \chi=\text{'}(n,i)\text{'}\\ 0, & \chi=\text{'}(n)\text{'}\end{cases}. \tag{25b}$$

4）Continuity of normal velocity at the boundary r_0=R_i:

For $-h<z<-d_0$

$$\frac{\partial \Phi_{N+1}^{\chi}\left(r_0,\theta_0,z\right)}{\partial r_0}=\frac{\partial \Phi_{0}^{\chi}\left(r_0,\theta_0,z\right)}{\partial r_0}. \tag{26a}$$

For $-d_0<z<0$

$$\frac{\partial \Phi_{N+1}^{\chi}\left(r_0,\theta_0,z\right)}{\partial r_0}=\begin{cases}-\dfrac{\partial \Phi_{\mathrm{I}}\left(r_0,\theta_0,z\right)}{\partial r_0}, & \chi=\text{'}(0)\text{'}\\ \delta_{n,0}\left[\delta_{1,i}\cos\theta_n+\delta_{2,i}\sin\theta_n\right. & \\ \quad\left.-\delta_{4,i}\left(z-z_n\right)\sin\theta_n+\delta_{5,i}\left(z-z_n\right)\cos\theta_n\right], & \chi=\text{'}(n,i)\text{'}\\ 0, & \chi=\text{'}(n)\text{'}\end{cases}. \tag{26b}$$

Upon substituting the diffracted and radiated spatial potentials in Eqs. (12)~(22) into Eqs. (23)~(26), utilizing the orthogonal properties of the functions cos$m\theta$, sin$m\theta$, and Z_l(z) (Zheng and Zhang, 2015; 2016), and making some rearrangements, the diffracted spatial potentials and the radiated ones in each subdomain can be obtained by solving a matrix equation, in which the infinite series are truncated by choosing (2M+1) terms (m=-M, …, 0, …, M) for $\mathrm{e}^{\mathrm{i}m\theta}$ functions and L_0+1 terms (l=0, 1, 2, … L_0) for Z_l(z) and cos[$\beta_{j,l}$(z+h)] functions. The brief derivation and the final complicated formulas for calculation of these unknown coefficients for wave diffraction as an example are given in Appendix A.

3.3 Wave excitation volume flux/forces

Wave excitation volume flux is the upward flux at the water surface inside the OWC chamber due to the contributions of undisturbed incident wave and the diffracted wave when the dynamic air pressure is zero. Expression of the wave excitation volume flux can be written as $\mathrm{Re}\left[F_\mathrm{e}^{(0)}\mathrm{e}^{-\mathrm{i}\omega t}\right]$, where, with utilization of Eq.(2) and Eq.(16),

$$\begin{aligned}F_\mathrm{e}^{(0)}&=\int_0^{2\pi}\int_0^{R_\mathrm{i}}\left.\frac{\partial\left(\Phi_{\mathrm{I}}+\Phi_{\mathrm{D},N+1}\right)}{\partial z}\right|_{z=0} r_0\mathrm{d}r_0\mathrm{d}\theta_0=\frac{\omega^2}{g}\int_0^{2\pi}\int_0^{R_\mathrm{i}}\left.\left(\Phi_{\mathrm{I}}+\Phi_{\mathrm{D},N+1}\right)\right|_{z=0} r_0\mathrm{d}r_0\mathrm{d}\theta_0\\&=\frac{2\pi\omega^2R_\mathrm{i}}{g}\left[-\frac{\mathrm{i}gA}{\omega}\frac{J_1\left(kR_\mathrm{i}\right)}{k}+\frac{D_{0,0}^{\mathrm{D},N+1}J_1\left(kR_\mathrm{i}\right)}{k_0J_0\left(kR_\mathrm{i}\right)}+\sum_{l=1}^{\infty}\frac{D_{0,l}^{\mathrm{D},N+1}I_1\left(k_lR_\mathrm{i}\right)}{k_lI_0\left(k_lR_\mathrm{i}\right)}\right]\end{aligned}. \tag{27}$$

Wave excitation forces are the forces due to the incident wave acting on structures which are stationary. It can be computed from the incident wave potential and the diffracted potential. Mode

j of the generalized excitation force on Float n is $\mathrm{Re}\left[F_{\mathrm{e}}^{n,j}\mathrm{e}^{-\mathrm{i}\omega t}\right]$, where

$$F_{\mathrm{e}}^{n,j}=-\mathrm{i}\omega\rho\int_{S_n}\left(\Phi_{\mathrm{I}}+\Phi_{\mathrm{D}}\right)n_j\mathrm{d}s\,, \tag{28}$$

in which S_n is the wet surface of Float n (n=0,2,3,…N); n_j represents the generalized normal with $n_1=n_x,\ n_2=n_y,\ n_3=n_z,\ n_4=-(z-z_n)n_y+yn_z,\ n_5=(z-z_n)n_x-(x-x_n)n_z,\ n_6=-yn_x+(x-x_n)n_y,\ \vec{n}=n_x\vec{i}+n_y\vec{j}+n_z\vec{k}$ is the unit normal vector pointing into the fluid domain at the considered float surface.

After inserting the theoretical expressions for the diffracted potentials as derived in Section 3.1 into Eq. (28), the wave excitation force exerting on Float n (n=0,2,3,…N) in different mode can be calculated directly.

3.4 Hydrodynamic coefficients

When the water column inside the chamber or the floats oscillate in the absence of an incident wave, the radiated wave reacts with an upward flux at the water surface inside the OWC chamber, so-called radiation volume flux, and forces on the floats, so-called radiation forces. The complex amplitudes of radiation volume flux due unit amplitude velocity oscillation of Float n (n=0,1,2,3,…N) oscillating in Mode i can be written into imaginary and real parts as:

$$\begin{aligned}F_{\mathrm{R},n,i}^{(0)}&=\int_0^{2\pi}\int_0^{R_{\mathrm{i}}}\left.\frac{\partial\Phi_{\mathrm{R}}^{n,i}}{\partial z}\right|_{z=0}r_0\mathrm{d}r_0\mathrm{d}\theta_0=\frac{\omega^2}{g}\int_0^{2\pi}\int_0^{R_{\mathrm{i}}}\left.\Phi_{\mathrm{R},N+1}^{(n,i)}\right|_{z=0}r_0\mathrm{d}r_0\mathrm{d}\theta_0\\&=\frac{2\pi\omega^2R_{\mathrm{i}}}{g}\left[\frac{D_{0,0}^{(n,i),N+1}J_1\left(kR_{\mathrm{i}}\right)}{k_0J_0\left(kR_{\mathrm{i}}\right)}+\sum_{l=1}^{\infty}\frac{D_{0,l}^{(n,i),N+1}I_1\left(k_lR_{\mathrm{i}}\right)}{k_lI_0\left(k_lR_{\mathrm{i}}\right)}\right]=\mathrm{i}\omega a_{n,i}^{(0)}-c_{n,i}^{(0)}\end{aligned} \tag{29}$$

where the hydrodynamic coefficients $a_{n,i}^{(0)}$ and $c_{n,i}^{(0)}$ are real and dependent on frequency ω, representing the hydrodynamic coupling between the floats and the oscillating pressure distribution of the air inside the OWC chamber.

Similarly, the complex amplitudes of radiation force exerting on Float n' (n'=0,1,2,3,…, N) in Mode i' due to unit amplitude velocity oscillation of Float n (n=0,1,2,3,…, N) oscillating in Mode i can be written in terms of hydrodynamic coefficients $a_{n,i}^{n',i'}$ and $c_{n,i}^{n',i'}$ as:

$$F_{\mathrm{R},n,i}^{(n',i')}=-\mathrm{i}\omega\rho\int_{S_{n'}}\Phi_{\mathrm{R}}^{n,i}n_{i'}\mathrm{d}s=\mathrm{i}\omega a_{n,i}^{n',i'}-c_{n,i}^{n',i'}\,, \tag{30}$$

where the hydrodynamic coefficients $a_{n,i}^{n',i'}$ and $c_{n,i}^{n',i'}$ are so-called added mass and radiation damping, respectively, representing the hydrodynamic coupling between the floats.

Similar expressions may be obtained for the complex amplitudes of radiation volume and the complex amplitude of radiation force exerting on Float n' (n'=0,1,2,3,…, N) in Mode i' due to unit air pressure oscillation inside the OWC chamber, and the corresponding hydrodynamic coefficients are denoted as $a_0^{(0)}$, $c_0^{(0)}$, and $a_0^{n',i'}$, $c_0^{n',i'}$, respectively.

The method for calculating the hydrodynamic coefficients as given in Eqs. (29) and (30) is straightforward based on the definitions of radiation volume flux and radiation forces. To distinguish this method with the others proposed below in Section 3.5, we call it “direct method”.

3.5 Hydrodynamic coefficients in terms of Far-Field Coefficients and wave excitation volume flux/forces

$c_0^{(0)}$ can be derived in terms of the radiated potential at infinity, the so-called Far-Field Coefficients.

For the wave radiated potential due to air pressure oscillation $\Phi_{\mathrm{R}}^{(0)}$ and its complex conjugate $\Phi_{\mathrm{R}}^{(0)*}$, both of them satisfy the Laplace equation within the fluid domain which is contained inside a closed surface composed of the internal water surface inside the OWC chamber, the free water surface external to the chamber and floats, the sum of all wet surfaces of OWC chamber and floats, the sea bed, and an envisaged vertical cylinder with a quite large radius. Hence Green's theorem is applicable to $\Phi_{\mathrm{R}}^{(0)}$ and $\Phi_{\mathrm{R}}^{(0)*}$,

$$\begin{aligned}&\iint_S\left(\Phi_{\mathrm{R}}^{(0)}\frac{\partial\Phi_{\mathrm{R}}^{(0)*}}{\partial n}-\Phi_{\mathrm{R}}^{(0)*}\frac{\partial\Phi_{\mathrm{R}}^{(0)}}{\partial n}\right)\mathrm{d}s\\&=\int_{S_{\mathrm{in}}}\left(\Phi_{\mathrm{R}}^{(0)}\frac{\partial\Phi_{\mathrm{R}}^{(0)*}}{\partial z}-\Phi_{\mathrm{R}}^{(0)*}\frac{\partial\Phi_{\mathrm{R}}^{(0)}}{\partial z}\right)\mathrm{d}s+\int_{S_\infty}\left(\Phi_{\mathrm{R}}^{(0)}\frac{\partial\Phi_{\mathrm{R}}^{(0)*}}{\partial r}-\Phi_{\mathrm{R}}^{(0)*}\frac{\partial\Phi_{\mathrm{R}}^{(0)}}{\partial r}\right)\mathrm{d}s,\\&=0\end{aligned}\tag{31}$$

where S represents the closed surface; S_∞ denotes the envisaged vertical cylinder with a extremely large radius $r_0=R_{\mathrm{f}}$; S_{in} denotes the internal water surface above the OWC. Note that the integrand vanishes on the sea bed, wet surfaces of fixed structures including OWC and floats, and free water surface, thus the integrand at these boundaries is not included in the second line of Eq.(31).

After inserting Eq. (9b) into Eq. (31), we have

$$\mathrm{Re}\int_{S_{\mathrm{in}}}\frac{\partial\Phi_{\mathrm{R}}^{(0)}}{\partial z}\mathrm{d}s-\rho\omega\,\mathrm{Im}\int_{S_\infty}\Phi_{\mathrm{R}}^{(0)}\frac{\partial\Phi_{\mathrm{R}}^{(0)*}}{\partial r}\mathrm{d}s=0,\tag{32}$$

Hence $c_0^{(0)}$ can be expressed by the radiated potential at extremely large distance as

$$c_0^{(0)}=-\mathrm{Re}\int_{S_{\mathrm{in}}}\frac{\partial\Phi_{\mathrm{R},0}^{(0)}}{\partial z}\mathrm{d}s=-\rho\omega\,\mathrm{Im}\int_{S_\infty}\Phi_{\mathrm{R}}^{(0)}\frac{\partial\Phi_{\mathrm{R}}^{(0)*}}{\partial r}\mathrm{d}s.\tag{33}$$

Using Graf's addition theorem to transform the diffracted potential in the outer ($r_0>R_{0j}$) regions in terms of the cylindrical coordinate systems $Or_0\theta_0$, and applying the asymptotic forms of H_m and H_m' as shown in Eq.(34),

$$H_m(x)=\sqrt{\frac{2}{\pi x}}\mathrm{e}^{\mathrm{i}\left(x-\frac{m\pi}{2}-\frac{\pi}{4}\right)},\qquad x\to\infty,\tag{34a}$$

$$H_m'(x)=\mathrm{i}\sqrt{\frac{2}{\pi x}}\mathrm{e}^{\mathrm{i}\left(x-\frac{m\pi}{2}-\frac{\pi}{4}\right)}=\mathrm{i}H_m(x),\qquad x\to\infty,\tag{34b}$$

we find that Eq. (33) becomes the expression of $c_0^{(0)}$ in terms of the Far-Field Coefficients as:

$$c_0^{(0)}=\frac{4\rho\omega h}{Z_0^2(0)}\mathrm{Re}\left\{\begin{aligned}&\sum_{m=-\infty}^{\infty}\left[\frac{\left|B_{m,0}^{(0),0}\right|^2}{\left|H_m\left(kR_0\right)\right|^2}\right]\\&+\sum_{m=-\infty}^{\infty}\sum_{j=1}^{N}\sum_{\tau=-\infty}^{\infty}J_{\tau-m}\left(kR_{j0}\right)\left[\frac{B_{m,0}^{(0),0}B_{\tau,0}^{(0),j*}\mathrm{e}^{\mathrm{i}(m-\tau)\alpha_{j0}}}{H_m\left(kR_0\right)H_\tau^*\left(kR_j\right)}+\frac{B_{m,0}^{(0),0*}B_{\tau,0}^{(0),j}\mathrm{e}^{\mathrm{i}(\tau-m)\alpha_{j0}}}{H_m^*\left(kR_0\right)H_\tau\left(kR_j\right)}\right]\\&+\sum_{j=1}^{N}\sum_{m=-\infty}^{\infty}\sum_{j'=1}^{N}\sum_{\tau=-\infty}^{\infty}\frac{B_{m,0}^{(0),j}B_{\tau,0}^{(0),j'*}}{H_m\left(kR_j\right)H_\tau^*\left(kR_j\right)}\sum_{m'=-\infty}^{\infty}J_{m-m'}\left(kR_{j0}\right)J_{\tau-m'}\left(kR_{j'0}\right)\mathrm{e}^{\mathrm{i}(m'-\tau)\alpha_{j'0}}\mathrm{e}^{\mathrm{i}(m-m')\alpha_{j0}}\end{aligned}\right\},\tag{35}$$

It is known that there is a Haskind relation between wave diffraction and radiation problems (Falnes, 2002), and therefore the hydrodynamic coefficients, such as $c_0^{(0)}$, $c_{n,i}^{n',i'}$ and $a_{n,i}^{(0)}$, $a_0^{n,i}$, can be written in terms of wave excitation volume flux and wave excitation forces as:

$$c_0^{(0)}=\frac{k}{8\pi\rho g v_{\mathrm{g}}A^2}\int_0^{2\pi}F_{\mathrm{e}}^{(0)}\left(\beta\right)F_{\mathrm{e}}^{(0)*}\left(\beta\right)\mathrm{d}\beta,\tag{36}$$

$$c_{n,i}^{n',i'}=\frac{k}{8\pi\rho g v_{\mathrm{g}}A^2}\int_0^{2\pi}F_{\mathrm{e}}^{n',i'}\left(\beta\right)F_{\mathrm{e}}^{n,i*}\left(\beta\right)\mathrm{d}\beta,\tag{37}$$

$$a_{n,i}^{(0)}=\frac{k\mathrm{i}}{8\pi\omega\rho g v_{\mathrm{g}}A^2}\int_0^{2\pi}F_{\mathrm{e}}^{(0)}\left(\beta\right)F_{\mathrm{e}}^{n,i*}\left(\beta\right)\mathrm{d}\beta,\tag{38a}$$

$$a_0^{n,i}=\frac{k\mathrm{i}}{8\pi\omega\rho g v_{\mathrm{g}}A^2}\int_0^{2\pi}F_{\mathrm{e}}^{n,i}\left(\beta\right)F_{\mathrm{e}}^{(0)*}\left(\beta\right)\mathrm{d}\beta,\tag{38b}$$

where v_{g} is the wave group velocity expressed as

$$v_{\mathrm{g}}=\frac{\omega}{2k}\left[1+\frac{2kh}{\sinh\left(2kh\right)}\right].\tag{39}$$

4. Wave power extraction

In this section, wave power extraction by the hybrid WEC is derived based on the coefficients obtained from the previous theoretical hydrodynamic model. Consider a hybrid WEC consisting of an OWC and N floats each hinged around by a rigid arm, as shown in Figure 1, the OWC chamber is assumed to be stationary here. Additionally, the density of each float is assumed half of the water density for a uniform distribution of the mass. Therefore, the centre of each float mass coincides well with the float geometry centre and they are all half submerged in still water.

Figure 3 gives plan view of the connection between the OWC and Float n (n=1, 2,…, N) in a more general hybrid WEC case. O_0xyz is the coordinate system of the OWC with O_0xy at the location of the mean water surface, the O_0z axis at the central axis of the OWC pointing upward and the O_0x axis pointing an arbitrary specified horizontal direction. $O_nx_ny_nz_n$ (n=1, 2,…, N) is the local coordinate system of Float n with $O_nx_ny_n$ at the location of the mean water surface, the O_nz_n axis at the central axis of Float n pointing upward and the O_nx_n in parallel with O_0x. The hinge for restricting Foat n is located h_n above the mean water surface. $O_{\mathrm{H}n}X_nY_nZ_n$ denotes the local coordinate system of the hinge for Float n with $O_{\mathrm{H}n}$ at the hinge location, $O_{\mathrm{H}n}X_n$ and $O_{\mathrm{H}n}Z_n$ pointing toward Float n horizontally and upward, respectively. The horizontal distance between

O_{Hn} and O_n is denoted as D_n. The relative angle between $O_{Hn}X_n$ and O_0x is denoted as α_{0n} (see Fig.3).

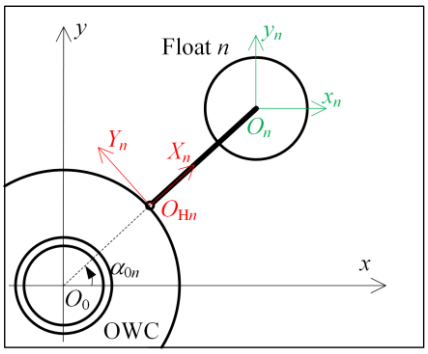

Fig. 3. Schematic of the connection between the OWC and Float *n* (plan view).

The force vector exerting on Float *n* in the local coordinate system $O_nx_ny_n$, denoted as $\boldsymbol{f}^{(n)}$, can be transformed into the corresponding rigid arm force vector in the $O_{Hn}X_nY_nZ_n$, denoted as $\boldsymbol{F}^{(n)}$, by using $\boldsymbol{F}^{(n)}=\mathbf{T}_{\mathrm{F}}^{(n)}\boldsymbol{f}^{(n)}$, where $\mathbf{T}_{\mathrm{F}}^{(n)}$ is the force transfer matrix and it is written as:

$$\mathbf{T}_{\mathrm{F}}^{(n)}=\begin{bmatrix} \cos\alpha_{0n} & \sin\alpha_{0n} & 0 & 0 & 0 & 0 \\ -\sin\alpha_{0n} & \cos\alpha_{0n} & 0 & 0 & 0 & 0 \\ 0 & 0 & 1 & 0 & 0 & 0 \\ -h_n\sin\alpha_{0n} & h_n\cos\alpha_{0n} & 0 & \cos\alpha_{0n} & \sin\alpha_{0n} & 0 \\ -h_n\cos\alpha_{0n} & -h_n\sin\alpha_{0n} & -D_n & -\sin\alpha_{0n} & \cos\alpha_{0n} & 0 \\ -D_n\sin\alpha_{0n} & D_n\cos\alpha_{0n} & 0 & 0 & 0 & 1 \end{bmatrix}. \tag{40}$$

In fact, the transfer matrix $\mathbf{T}_{\mathrm{F}}^{(n)}$ can also be used to obtain the displacement vector of Float *n* in the local coordinate system $O_nx_ny_n$, denoted as $\boldsymbol{x}^{(n)}$, from the corresponding rigid arm displacement vector in the $O_{Hn}X_nY_nZ_n$, denoted as $\boldsymbol{X}^{(n)}$, by $\boldsymbol{x}^{(n)}=\mathbf{T}_{\mathrm{F}}^{(n)}\boldsymbol{X}^{(n)}$.

4.1 Power take-off by the hybrid WEC

Assuming the chamber air to be compressible and its motion isentropic, then the effect of the linear air turbine and air compressibility in the chamber are linear as well, which can be characterized as a damping and added mass, respectively (Lovas et al. 2010; Martins-rivas and Mei, 2009a). After obtaining the wave excitation volume flux/forces, hydrodynamic coefficients and transforming these coefficients from the local coordinate system of Float *n* into the local coordinate system of the *n*-th hinge for Float *n*, the response of the hybrid WEC in frequency domain can be evaluated by using the dynamic motion matrix equation:

$$\left[-\mathrm{i}\omega\left(\mathbf{A}_{\mathrm{J}}\mathbf{T}_{\mathrm{F}}\mathbf{M}_{\mathrm{a}}\mathbf{T}_{\mathrm{F}}^{\mathrm{T}}\mathbf{A}_{\mathrm{J}}^{\mathrm{T}}+\mathbf{M}_{\mathrm{PTO}}+\mathbf{M}\right)+\left(\mathbf{A}_{\mathrm{J}}\mathbf{T}_{\mathrm{F}}\mathbf{C}_{\mathrm{d}}\mathbf{T}_{\mathrm{F}}^{\mathrm{T}}\mathbf{A}_{\mathrm{J}}^{\mathrm{T}}+\mathbf{C}_{\mathrm{PTO}}\right)+\mathrm{i}\mathbf{K}_{\mathrm{s}}/\omega\right]\dot{\boldsymbol{X}}=\mathbf{A}_{\mathrm{J}}\mathbf{T}_{\mathrm{F}}\boldsymbol{F}_{\mathrm{e}} \quad ,. \tag{41}$$

where $\boldsymbol{F}_{\mathrm{e}}$ is the wave excitation volume flux/force vector; $\mathbf{M}_{\mathrm{a}}$ and $\mathbf{C}_{\mathrm{d}}$ are the matrices of

hydrodynamic mass and damping, respectively; $\mathbf{M}$ and $\mathbf{K}_s$ are the WEC mass matrix and restoring stiffness matrix, respectively; $\mathbf{M}_{PTO}$ and $\mathbf{C}_{PTO}$ are the mass and damping matrices of the PTO system, respectively, in which the terms regarding to OWC come from (Lovas et al. 2010; Martins-rivas and Mei, 2009a) and they are given based on the assumption that the mass flux through the turbines is proportional to the chamber air pressure; $\mathbf{T}_F$ is the transfer matrix that is composed of $\mathbf{T}_F^{(n)}$; $\mathbf{A}_J$ is a constraint matrix that can be used to reduce the matrix order from $6N+1$ to $N+1$; $\dot{\boldsymbol{X}} = \begin{bmatrix} \dot{X}_0 & \dot{X}_1 & \dot{X}_2 & \cdots & \dot{X}_N \end{bmatrix}^{\mathrm{T}}$ is the velocity vector of the hybrid WEC, in which $\dot{X}_0 = p$ is the complex air pressure amplitude inside the OWC chamber, $\dot{X}_n$ represents the rotary velocity of Float n relative to the OWC. Among these matrices, $\boldsymbol{F}_e$, $\mathbf{M}_a$ and $\mathbf{C}_d$ are obtained from the theoretical hydrodynamic model built in Sections 2 and 3. Expressions of $\mathbf{M}$, $\mathbf{K}_s$, $\mathbf{M}_{PTO}$, $\mathbf{C}_{PTO}$, $\mathbf{T}_F$ and $\mathbf{A}_J$, are given as follows:

$$\mathbf{M} = \begin{bmatrix} 0 & & & & \\ & I_1 & & & \\ & & I_2 & & \\ & & & \ddots & \\ & & & & I_N \end{bmatrix}_{(N+1)\times(N+1)}, \quad I_n = \frac{\rho\pi R_n^2 d_n}{12}\left(3R_n^2 + 4d_n^2\right) + \rho\pi R_n^2 d_n\left(D_n^2 + h_n^2\right),$$

$$\mathbf{K}_s = \rho g \begin{bmatrix} 0 & & & & \\ & K_1 & & & \\ & & K_2 & & \\ & & & \ddots & \\ & & & & K_N \end{bmatrix}_{(N+1)\times(N+1)}, \quad K_n = \frac{\pi R_n^4}{4} + \pi R_n^2 D_n^2 - \pi R_n^2 \frac{d_n^2}{2},$$

$$\mathbf{M}_{PTO} = \begin{bmatrix} \frac{V_0}{c_a^2 \rho_0} & & & & \\ & 0 & & & \\ & & 0 & & \\ & & & \ddots & \\ & & & & 0 \end{bmatrix}_{(N+1)\times(N+1)}, \quad \mathbf{C}_{PTO} = \begin{bmatrix} c_0 & & & & \\ & c_1 & & & \\ & & c_2 & & \\ & & & \ddots & \\ & & & & c_N \end{bmatrix}_{(N+1)\times(N+1)},$$

$$\mathbf{T}_F = \begin{bmatrix} 1 & & & & \\ & \mathbf{T}_F^{(1)} & & & \\ & & \mathbf{T}_F^{(2)} & & \\ & & & \ddots & \\ & & & & \mathbf{T}_F^{(N)} \end{bmatrix}_{(6N+1)\times(6N+1)},$$

$$\mathbf{A}_{\mathrm{J}}=\begin{bmatrix}1 & & & & \\ & \mathbf{R} & & & \\ & & \mathbf{R} & & \\ & & & \ddots & \\ & & & & \mathbf{R}\end{bmatrix}_{(N+1)\times(6N+1)},\quad \mathbf{R}=\begin{bmatrix}0 & 0 & 0 & 0 & 1 & 0\end{bmatrix},$$

where c_n represents the damping coefficient in the PTO system of the OWC (n=0) and Float n (n=1, 2, …, N), c_a is the sound velocity in air, ρ_0 is the static air density, V_0 is the air chamber volume. Following the previous study carried out by Lovas et al. (2010), Martins-rivas and Mei (2009a), ρ/ρ_0=1000, c_a=340 m/s and $V_0=\pi R_1^2 d_0$ are employed in subsequent computations, although these adopted value might be unrealistic for atmospheric pressure at sea level.

The average power that the hybrid WEC captures from regular waves can be written as:

$$P=\frac{1}{2}\dot{\boldsymbol{X}}^{*}\mathbf{C}_{\mathrm{PTO}}\dot{\boldsymbol{X}}\,. \tag{42}$$

The average wave energy capture width ratio (or capture factor) η is calculated as:

$$\eta=\frac{kP}{2\pi P_{\mathrm{in}}}, \tag{43}$$

where P_{in} represents the incoming wave power per unit width of the wave front given by:

$$P_{\mathrm{in}}=\frac{\rho g H^2}{8}\frac{\omega}{2k}\left[1+\frac{2kh}{\sinh\left(2kh\right)}\right], \tag{44}$$

in which H represent the wave height of incident waves.

As Ricci et al. (2007) reported, no significant improvement can be obtained by individually optimizing the PTO coefficients of each device in an array. Thus in the cases studied in the present paper, the PTO damping (c_n) is the same for all the hinged floats.

The dimensionless quantities of the PTO damping of the OWC and the hinged floats (c_0 and c_1) are defined by:

$$\overline{c}_0=\frac{\rho g c_0}{h\sqrt{gh}},\quad \overline{c}_1=\frac{c_1}{\rho h^4\sqrt{gh}}. \tag{45}$$

As the PTO damping of both the OWC and the hinged floats (c_0 and c_1) change from 0 to $+\infty$, there will be an optimized combination of damping coefficients, denoted as ($c_{\mathrm{opt}}^{(0)}$ and $c_{\mathrm{opt}}^{(1)}$), to maximize the power absorbed by the hybrid WEC. The maximum absorbed power and the corresponding maximum power capture factor are denoted as $P_{\max}$ and $\eta_{\max}$, respectively.

In the case of WEC arrays, a parameter named q-factor, which denotes the ratio of the powers absorbed by the array in whole and by the isolated device in summary, is generally used to measure the effect of hydrodynamic interactions between the devices (Borgarino et al., 2012; Babarit, 2013; Penalba et al., 2017b). q-factor can also be employed as a reference value to assess the performance of the hybrid WEC. For the hybrid WEC, the definition of the q-factor is modified as the maximum power absorbed by the hybrid WEC dividing the sum of the maximum

power absorptions of the isolated OWC and the array of hinged floats in absence of the OWC. When q>1, the maximum power absorption of the hybrid WEC is larger than that of an isolated OWC together with that of the hinged floats, and it means that the interaction between the OWC and the floats has positive effects. On the contrary, when q<1, the interaction is negative.

4.2 Power take-off by an isolated OWC

For an isolated OWC, as shown in Fig. 4, assuming the OWC chamber is stationary due to the restricts by the mooring lines, response of the dynamic air pressure in frequency domain can be easily evaluated by using the one degree motion equation:

$$\left[-\mathrm{i}\omega\left(\tilde{m}_{\mathrm{a}}+\tilde{m}_{\mathrm{PTO}}\right)+\left(\tilde{c}_{\mathrm{d}}+\tilde{c}_{\mathrm{PTO}}\right)\right]\tilde{p}=\tilde{F}_{\mathrm{e}}^{(0)}, \tag{46}$$

where $\omega\tilde{m}_{\mathrm{a}}$ and $\tilde{c}_{\mathrm{d}}$ are so-called the radiation susceptance and the radiation conductance of the isolated OWC, respectively; $\tilde{m}_{\mathrm{PTO}}=V_0\big/\left(c_{\mathrm{a}}^2\rho_0\right)$ and $\tilde{c}_{\mathrm{PTO}}$ are the mass and damping induced by the PTO system; $\tilde{p}$ and $\tilde{F}_{\mathrm{e}}^{(0)}$ represent the dynamic air pressure and excitation volume flux of the OWC separately. The hydrodynamic coefficients of the isolated OWC, i.e. $\tilde{m}_{\mathrm{a}}$, $\tilde{c}_{\mathrm{d}}$ and $\tilde{F}_{\mathrm{e}}^{(0)}$ can also be calculated using the theoretical hydrodynamic model built in Sections 2 and 3 when the number of floats N=0 is implemented.

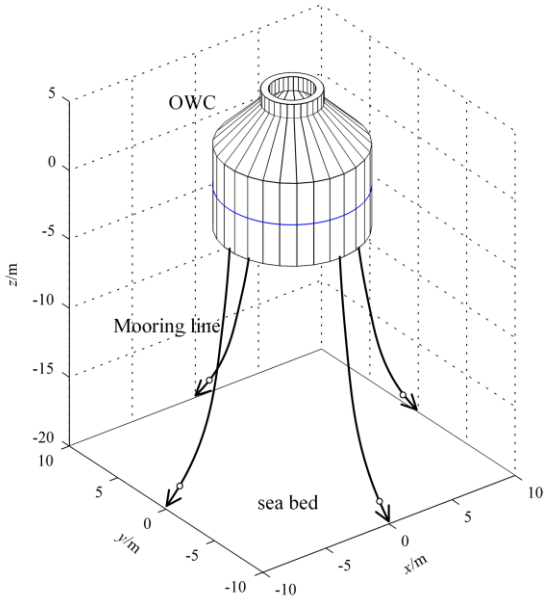

Fig. 4. Sketch of an isolated OWC device

After solving Eq. (46), the average power absorbed by the OWC, denoting as $\tilde{P}$, can be expressed as:

$$\tilde{P}=\frac{1}{2}\tilde{p}^{*}\tilde{c}_{\mathrm{PTO}}\tilde{p}=\frac{1}{2}\frac{\tilde{c}_{\mathrm{PTO}}\left|\tilde{F}_{\mathrm{e}}^{(0)}\right|^2}{\omega^2\left(\tilde{m}_{\mathrm{a}}+\tilde{m}_{\mathrm{PTO}}\right)^2+\left(\tilde{c}_{\mathrm{d}}+\tilde{c}_{\mathrm{PTO}}\right)^2}. \tag{47}$$

There is a maximum of absorbed power when $\partial\tilde{P}/\partial\tilde{c}_{\mathrm{PTO}}=0$, which occurs if

$$\tilde{c}_{\mathrm{opt}}=\sqrt{\tilde{c}_{\mathrm{d}}^2+\omega^2\left(\tilde{m}_{\mathrm{a}}+\tilde{m}_{\mathrm{PTO}}\right)^2}\,, \tag{48}$$

for which the corresponding maximum absorbed power is

$$\tilde{P}_{\max}=\frac{1}{4}\frac{\left|\tilde{F}_{\mathrm{e}}^{(0)}\right|^2}{\tilde{c}_{\mathrm{d}}+\sqrt{\tilde{c}_{\mathrm{d}}^2+\omega^2\left(\tilde{m}_{\mathrm{a}}+\tilde{m}_{\mathrm{PTO}}\right)^2}}. \tag{49}$$

4.3 Power take-off by an array of hinged floats

As shown in Fig. 5, after removing the OWC from the hybrid WEC, the rest *N* floats can also be used to extract wave power if they are hinged on *N* legs standing on the seabed.

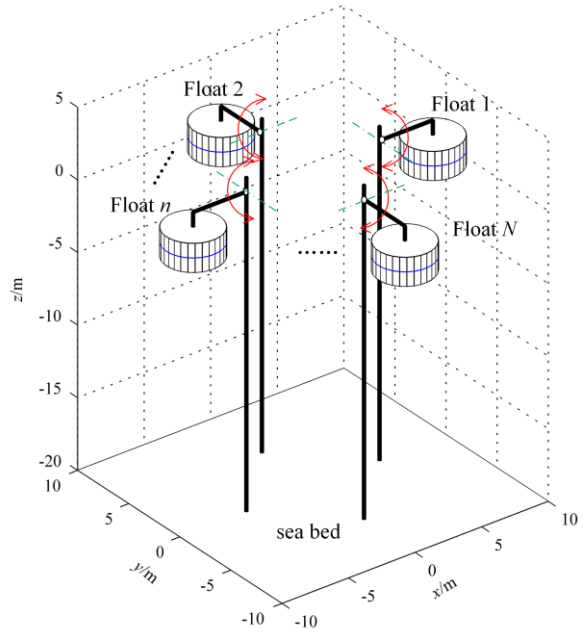

Fig. 5. Sketch of an array of four hinged floats

Similar to Eq.(41), response equation of the *N* floats, as shown in Fig.5, in frequency domain can be written as:

$$\left[-\mathrm{i}\omega\left(\hat{\mathbf{A}}_{\mathrm{J}}\hat{\mathbf{T}}_{\mathrm{F}}\hat{\mathbf{M}}_{\mathrm{a}}\hat{\mathbf{T}}_{\mathrm{F}}^{\mathrm{T}}\hat{\mathbf{A}}_{\mathrm{J}}^{\mathrm{T}}+\hat{\mathbf{M}}\right)+\left(\hat{\mathbf{A}}_{\mathrm{J}}\hat{\mathbf{T}}_{\mathrm{F}}\hat{\mathbf{C}}_{\mathrm{d}}\hat{\mathbf{T}}_{\mathrm{F}}^{\mathrm{T}}\hat{\mathbf{A}}_{\mathrm{J}}^{\mathrm{T}}+\hat{\mathbf{C}}_{\mathrm{PTO}}\right)+\mathrm{i}\hat{\mathbf{K}}_{\mathrm{s}}/\omega\right]\dot{\boldsymbol{X}}_{\mathrm{floats}}=\hat{\mathbf{A}}_{\mathrm{J}}\hat{\mathbf{T}}_{\mathrm{F}}\hat{\boldsymbol{F}}_{\mathrm{e}}\,, \tag{50}$$

in which $\hat{\boldsymbol{F}}_{\mathrm{e}}$ is the wave excitation force vector; $\hat{\mathbf{M}}_{\mathrm{a}}$ and $\hat{\mathbf{C}}_{\mathrm{d}}$ are the matrices of added-mass and wave radiation damping, respectively; $\hat{\mathbf{M}}$ and $\hat{\mathbf{K}}_{\mathrm{s}}$ are mass matrix and restoring stiffness matrix, respectively, of the *N* floats; $\hat{\mathbf{C}}_{\mathrm{PTO}}$ is the damping matrices of the PTO system, respectively; $\hat{\mathbf{T}}_{\mathrm{F}}$ is the transfer matrix; $\hat{\mathbf{A}}_{\mathrm{J}}$ is a constraint matrix to reduce the matrix order from 6*N* to *N*; $\dot{\boldsymbol{X}}_{\mathrm{floats}}=\left[\dot{X}_1\quad\dot{X}_2\quad\cdots\quad\dot{X}_N\right]^{\mathrm{T}}$ is the velocity vector of the *N* floats. $\hat{\boldsymbol{F}}_{\mathrm{e}}$, $\hat{\mathbf{M}}_{\mathrm{a}}$

and $\hat{\mathbf{C}}_{\mathrm{d}}$ can be obtained with the implement of the theoretical hydrodynamic model proposed by Siddorn and Eatock Taylor (2008).

In the absence of the OWC, the power absorbed by the hinged floats, as shown in Fig. 5, can be written as:

$$\hat{P}=\frac{1}{2}\dot{\boldsymbol{X}}^{*}_{\mathrm{floats}}\hat{\mathbf{C}}_{\mathrm{PTO}}\dot{\boldsymbol{X}}_{\mathrm{floats}}=\frac{\hat{c}_{\mathrm{PTO}}}{2}\dot{\boldsymbol{X}}^{*}_{\mathrm{floats}}\dot{\boldsymbol{X}}_{\mathrm{floats}}, \tag{51}$$

where the second equality sign is valid when the PTO damping of each float is all the same as, $c_n=\hat{c}_{\mathrm{PTO}}$ (n=1,2, ……, N). The maximum power absorption, $\hat{P}_{\max}$, and the corresponding optimal PTO damping, $\hat{c}_{\mathrm{opt}}$, can be obtained using trial-and-error method.

For any specified hybrid WEC, once $P_{\max}$, $\tilde{P}_{\max}$ and $\hat{P}_{\max}$ are obtained, the q-factor can be then calculated as:

$$q=\frac{P_{\max}}{\tilde{P}_{\max}+\hat{P}_{\max}}. \tag{52}$$

5 Results and discussion

5.1 Validation of the theoretical hydrodynamic model

To validate the above-derived theoretical hydrodynamic model for diffracted and radiated spatial potentials as given in Sections 2 and 3, wave excitation volume flux of the OWC, wave excitation forces exerting on different floats and hydrodynamic coefficients are calculated by using the present theoretical method and a numerical computational fluid dynamics model based on the boundary element method package of ANSYS AQWA. The numerical CFD analysis only deals with the homogeneous boundary for free water surface and it works well in solving wave diffraction problem from the hybrid WEC, while the boundary condition at internal water surface of the OWC due to dynamic air pressure is inhomogeneous, hence hydrodynamic coefficients related to the radiation induced by OWC air pressure oscillation cannot be directly obtained with numerical method. Apart from numerical method, the different theoretical approaches for evaluating hydrodynamic coefficients can also be used to check the validity of the present theoretical hydrodynamic model.

We consider four truncated floats with different radius and draft employed around an OWC, as illustrated in Fig. 6. All of these structures are half submerged in the water. Table 1 gives a list of the dimensions of the OWC and floats. In addition, the water depth h is 20m; the inner radius of the OWC R_{i}=4.0m; the sea water density ρ=1025kg/m^3; wave incoming direction β=π/8; the acceleration of gravity g =9.81 m/s^2. The reference rotation center of each float is set to (0, 0) in their own local cylindrical coordinate systems.

Table 1 Basic parameters of the OWC and floats as shown in Fig. 6. (Units: m)

	OWC	Float 1	Float 2	Float 3	Float 4
Centre position, (x_n, y_n)	(0, 0)	(-7.0, 7.0)	(7.0, -7.0)	(-7.0, -7.0)	(7.0, 7.0)
Radius, R_n	5.0	1.0	1.0	2.0	1.5
draft, d_n	3.0	2.0	1.0	2.5	1.0

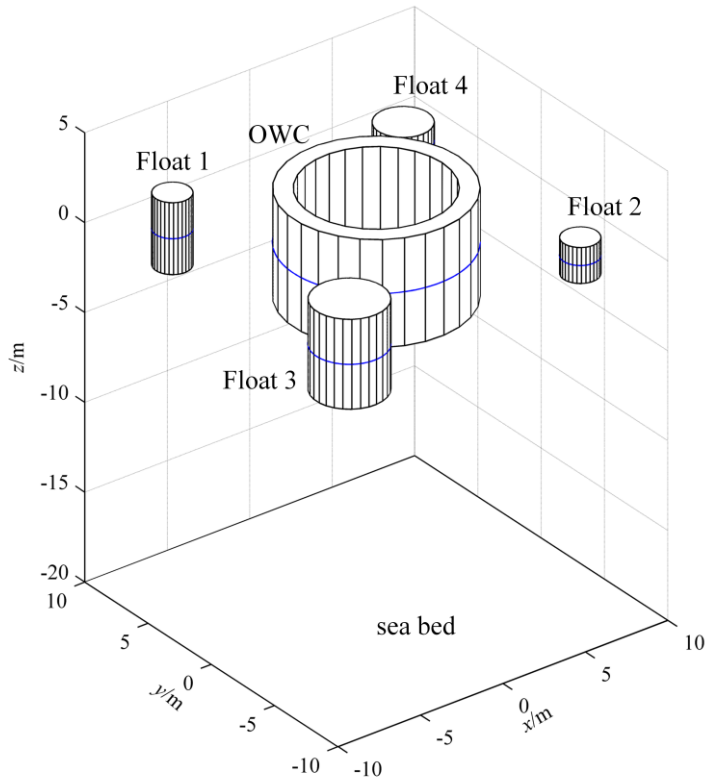

Fig. 6. The case consisting of an OWC and four floats around.

The dimensionless quantities of the wave excitation volume flux/forces and hydrodynamic coefficients are defined by:

$$\bar{F}_{\mathrm{e}}^{n,i}=\frac{\left|F_{\mathrm{e}}^{n,i}\right|}{\rho g R_0^j A};\quad \varphi_{\mathrm{e}}^{n,i}=\arg F_{\mathrm{e}}^{n,i};\quad \bar{F}_{\mathrm{e}}^{(0)}=\frac{\omega\left|F_{\mathrm{e}}^{(0)}\right|}{gR_0A};\quad \varphi_{\mathrm{e}}^{(0)}=\arg F_{\mathrm{e}}^{(0)}, \tag{53a}$$

where j=2 for i =1~3; whereas j=3 for i =4~5.

$$\bar{a}_{n,i}^{n',i'}=\frac{a_{n,i}^{n',i'}}{\rho R_0^j};\quad \bar{c}_{n,i}^{n',i'}=\frac{c_{n,i}^{n',i'}}{\omega\rho R_0^j};\quad \bar{a}_0^{(0)}=\frac{\omega^2\rho a_0^{(0)}}{R_0};\quad \bar{c}_0^{(0)}=\frac{\omega\rho c_0^{(0)}}{R_0}, \tag{53b}$$

where j=3 for (i, i')=(1~3, 1~3); j=4 for (i, i')=(1~3, 4~5) and (4~5, 1~3); whereas j=5 for (i, i')=(4~5, 4~5).

$$\bar{a}_0^{n,i}=\frac{\omega a_0^{n,i}}{R_0^j};\quad \bar{c}_0^{n,i}=\frac{c_0^{n,i}}{R_0^j};\quad \bar{a}_{n,i}^{(0)}=\frac{\omega a_{n,i}^{(0)}}{R_0^j};\quad \bar{c}_{n,i}^{(0)}=\frac{c_{n,i}^{(0)}}{R_0^j}, \tag{53c}$$

where j=2 for i =1~3; whereas j=3 for i =4~5.

In our theoretical computations for the case as given in Fig.6 and Table 1 , to obtain converged results using the eigen-series analysis described above, we found it necessary to take M=12, L_0=20 through theoretical experiments. Theoretical and numerical results for the case are presented below.

Wave diffraction problem

Figure 7 shows variation of the computed wave excitation volume flux of the OWC in terms of amplitude and phase with wave number for $\beta=\pi/8$. As given in Fig. 7a, the theoretical results

and the numerical ones for $\bar{F}_{\mathrm{e}}^{(0)}$ generally agree quite well with each other, and there is one maximum of $\bar{F}_{\mathrm{e}}^{(0)}$ at kR_0=1.0 in the computed range of kR_0, which is associated with the fundamental resonance inside the OWC chamber. The agreement between the theoretical and numerical results can also be found for $\varphi_{\mathrm{e}}^{(0)}$, as shown in Fig. 7b, especially when kR_0<6.0. For kR_0>6.0, wave excitation volume flux of the OWC is too small ($\bar{F}_{\mathrm{e}}^{(0)}$<0.005) thus the differences between the results of $\varphi_{\mathrm{e}}^{(0)}$ using different methods could be reasonably induced by error amplification. Due to the small value of $\bar{F}_{\mathrm{e}}^{(0)}$ ($\bar{F}_{\mathrm{e}}^{(0)}$<0.005) for kR_0>6.0, the corresponding value of $\varphi_{\mathrm{e}}^{(0)}$ affects the hydrodynamic problem quite little.

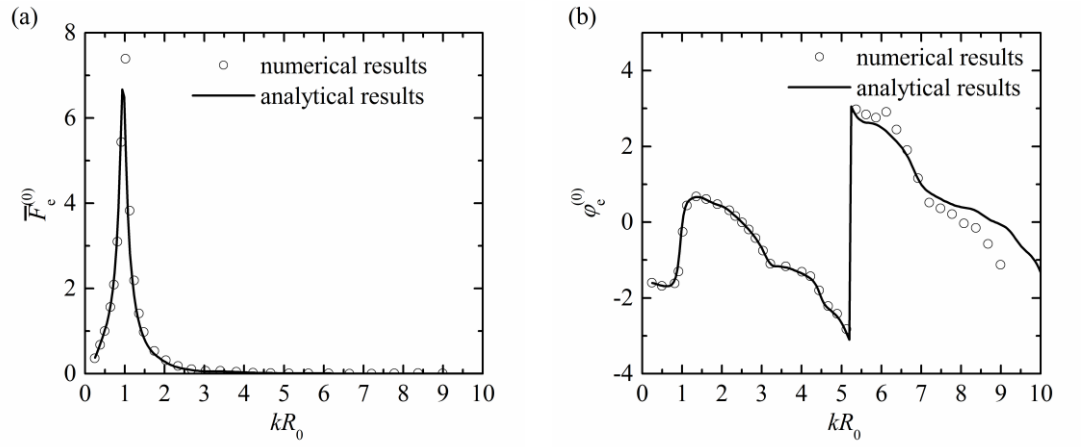

Fig. 7. Wave excitation volume flux of the OWC for $\beta=\pi/8$. a) $\bar{F}_{\mathrm{e}}^{(0)}$; b) $\varphi_{\mathrm{e}}^{(0)}$.

Figures 8 and 9 illustrate the wave excitation forces exerting on Float 0 (OWC) and Floats 1~4, respectively, in surge, sway and heave for $\beta=\pi/8$. The theoretical results agree quite well with the numerical ones in terms of both the amplitude and the phase of wave excitation forces. As given in Fig.8, there are sharp changes of the surge and heave excitation forces exerting on the OWC, which occur at kR_0=2.4 and 1.0, respectively. Because of the larger scale of Float 3 in both radius and draft compared with the other floats, for most wave conditions as shown in Fig. 9, the wave excitation forces exerting on Float 3 in surge, sway and heave hold the largest value. As wave number $kR_0\to 0$, the heave wave excitation force exerting on Float n, $F_{\mathrm{e}}^{n,3}\to\pi\rho g R_n^2 A$, resulting in $\bar{F}_{\mathrm{e}}^{n,3}\to\pi R_n^2/R_0^2$. Thus $\bar{F}_{\mathrm{e}}^{n,3}$=0.126, 0.126, 0.503 and 0.283, respectively, at $kR_0\to 0$ for Floats 1~4, which can be seen from Fig.9e as well. It can also be observed from Figs. 9b, 9d and 9f that the phase of wave excitation forces exerting on Float 3 and Float 4 changes more rapidly with kR_0 than those for Float 1 and Float 2. This might be explained by the fact that the incident and diffracted waves act on the float simultaneously, and minor change in the incident wave frequency will lead to a larger phase difference between those two waves for a larger

spacing distance along wave propagating direction. As wave incident angle $\beta=\pi/8$, thus the spacing distance between Floats 1 (and Float 2) and the OWC projected to the wave propagating direction is smaller than that for Float 3 (and Float 4), therefore a smaller frequency oscillation of the $\varphi_e^{n,i}$-kR_0 curve is obtained for Floats 1 (and Float 2). Figure 9 also shows that, due to the OWC resonance at $kR_0=1.0$, sharp changes of the wave excitation forces occur around $kR_0=1.0$ for all the floats.

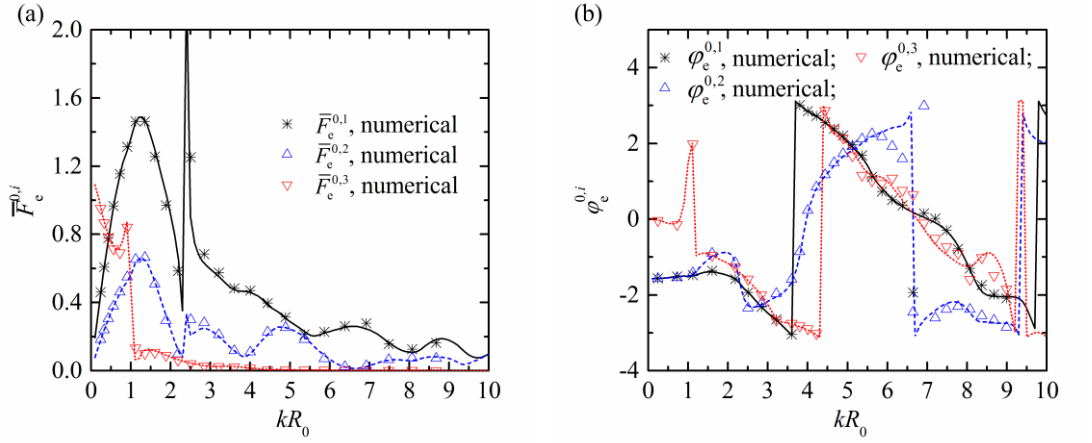

Fig. 8. Wave excitation forces exerting on Float 0 (OWC) in surge, sway and heave modes for $\beta=\pi/8$. a) $\overline{F}_e^{0,i}$; b) $\varphi_e^{0,i}$. solid line: theoretical results for surge mode; dash line: theoretical results for sway mode; dot line: theoretical results for heave mode.

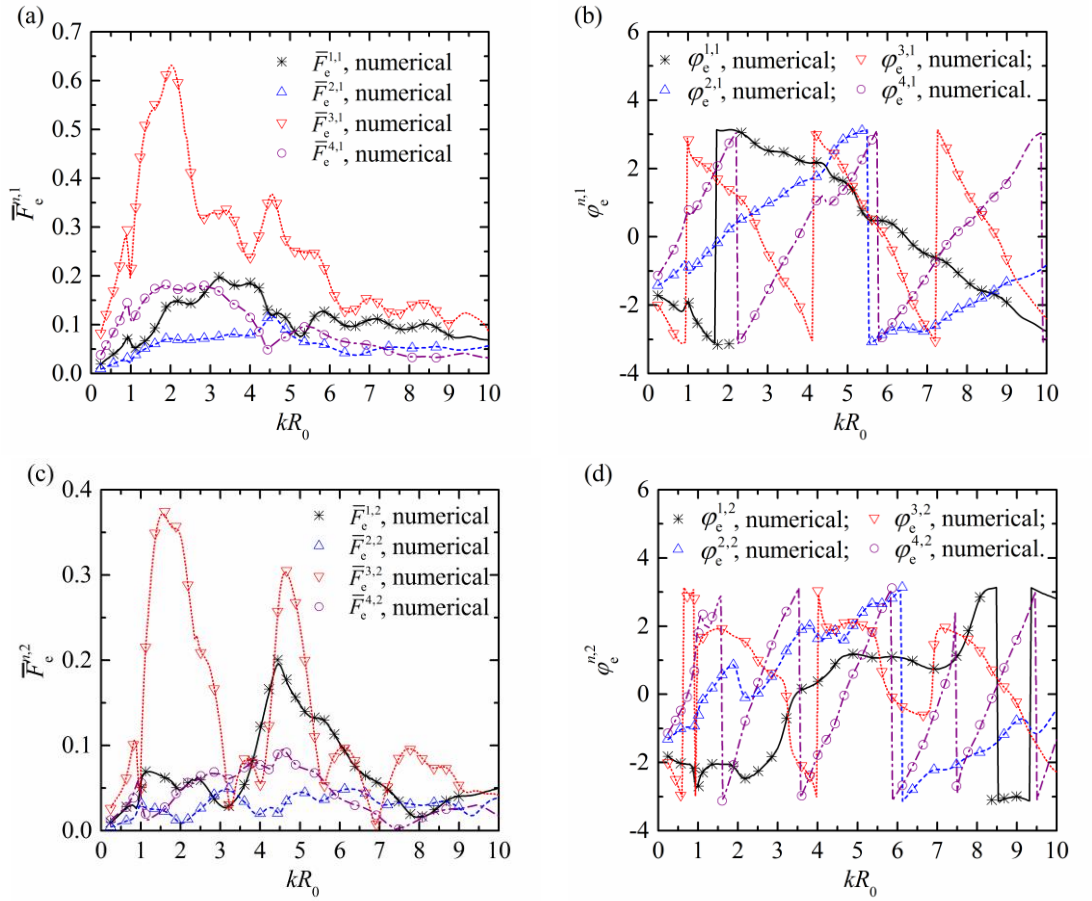

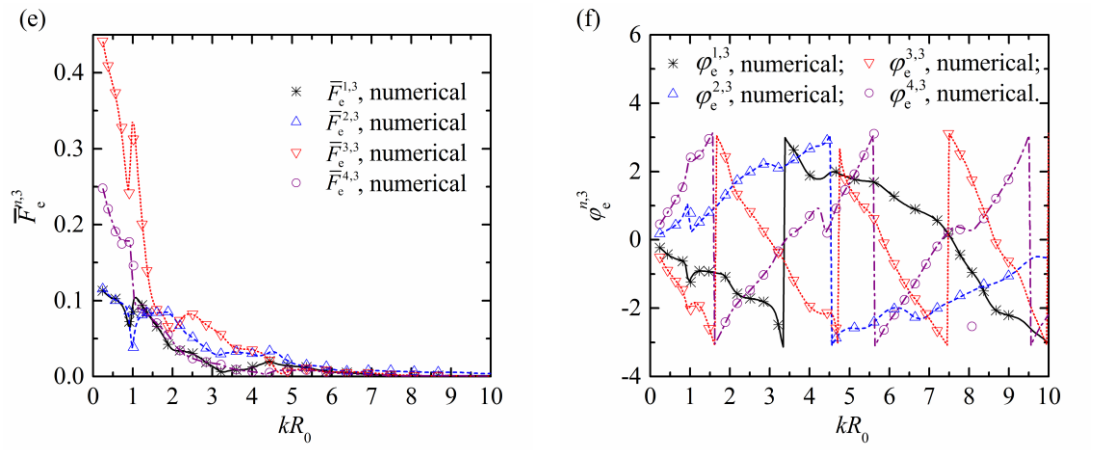

Fig. 9. Wave excitation forces exerting on Floats 1~4 in surge, sway and heave modes for $\beta=\pi/8$. a) $\bar{F}_e^{n,1}$; b) $\varphi_e^{n,1}$; c) $\bar{F}_e^{n,2}$; d) $\varphi_e^{n,2}$; e) $\bar{F}_e^{n,3}$; f) $\varphi_e^{n,3}$. solid line: theoretical results for Float 1; dash line: theoretical results for Float 2; dot line: theoretical results for Float 3; dash dot line: theoretical results for Float 4.

The agreement of the present theoretical results of both $F_e^{(0)}$ and $F_e^{n,j}$ with those obtained by numerical method illustrates that the diffraction problem is solved correctly.

Wave radiation problem

To verify the correctness of the expressions for the radiated potentials, here, hydrodynamic coefficients of the OWC due to the oscillating air pressure inside the OWC chamber, hydrodynamic coefficients of the float due to the oscillation of itself and the other floats, and hydrodynamic coefficients due to hydrodynamic interaction between the OWC and floats are all computed using different methods, and these results are also compared with each other obtained by using different method.

Figure 10 gives the results of hydrodynamic coefficients of the OWC due to the oscillating air pressure inside the OWC chamber. It can be learnt from Fig.10a that the $\bar{a}_0^{(0)}$-kR_0 curve shapes like the letter N and $\bar{a}_0^{(0)}$ rapidly changes sign around the resonance frequency kR_0=1.0. The theoretical results of $\bar{c}_0^{(0)}$ by adopting three different approaches as presented in Sections 3.4 and 3.5, i.e., direct method, expressions in terms of Far Field Coefficient and those based on Haskind Relation, are plotted in Fig.10b, which agree quite well with each other. A sharp peak of $\bar{c}_0^{(0)}$ with the value of 22.5 occurs at kR_0=1.0.

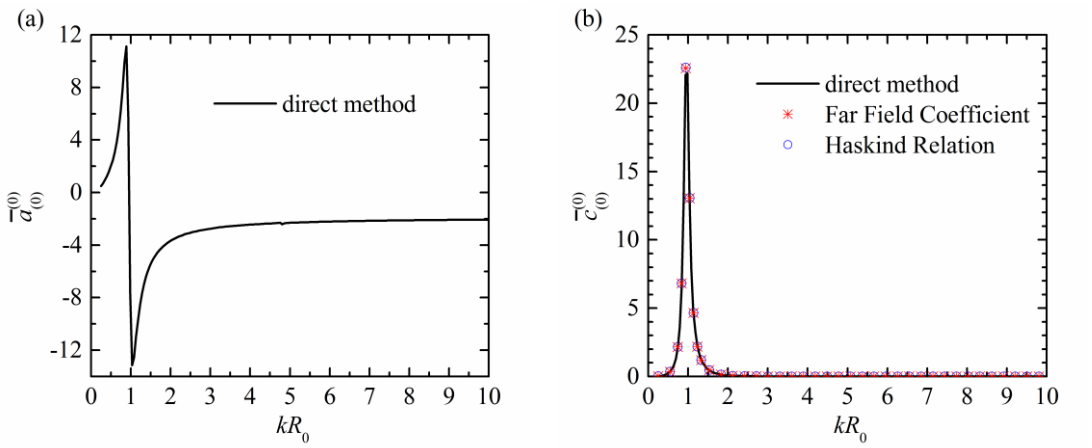

Fig. 10. Hydrodynamic coefficients of the OWC due to the oscillating air pressure inside the OWC chamber. a) $\overline{a}_0^{(0)}$; b) $\overline{c}_0^{(0)}$.

Figures 11 and 12 present both theoretical and numerical results of the hydrodynamic coefficients of Float 0 (OWC) and Float 1 due to the oscillation of themselves. The results for hydrodynamic coefficients obtained by using the present theoretical method and the numerical method agree well with each other.

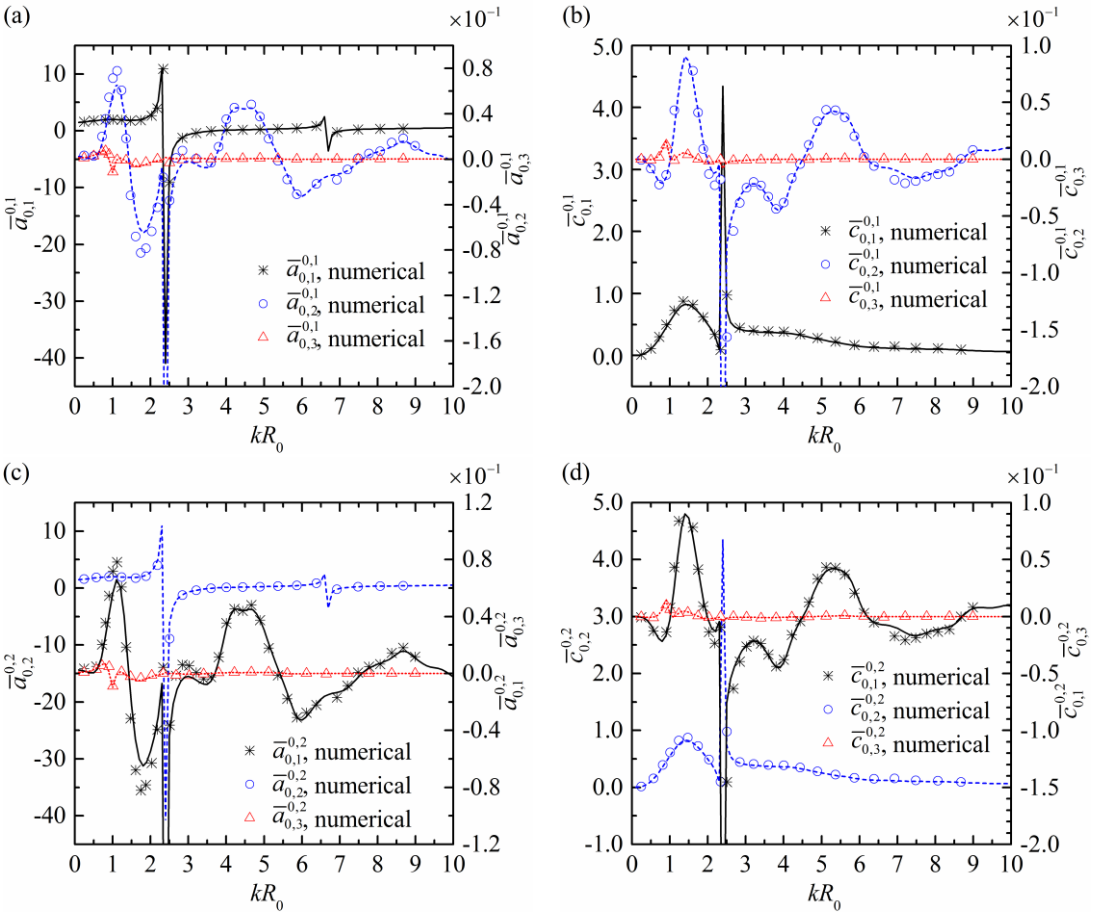

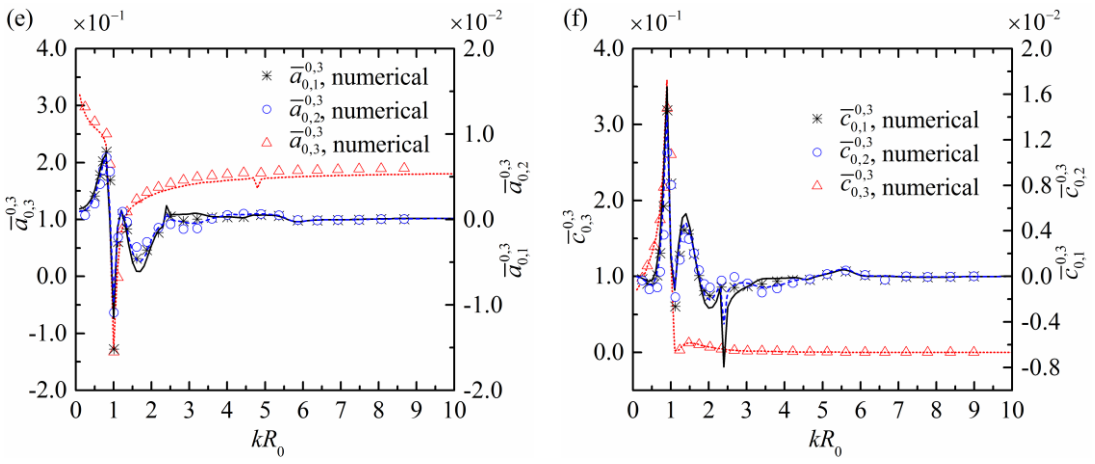

Fig. 11. Hydrodynamic coefficients of Float 0 (OWC) due to its oscillation. a) $\bar{a}_{0,i}^{0,1}$; b) $\bar{c}_{0,i}^{0,1}$; c) $\bar{a}_{0,i}^{0,2}$; d) $\bar{c}_{0,i}^{0,2}$; e) $\bar{a}_{0,i}^{0,3}$; f) $\bar{c}_{0,i}^{0,3}$. solid line, dash line and dot line: theoretical results.

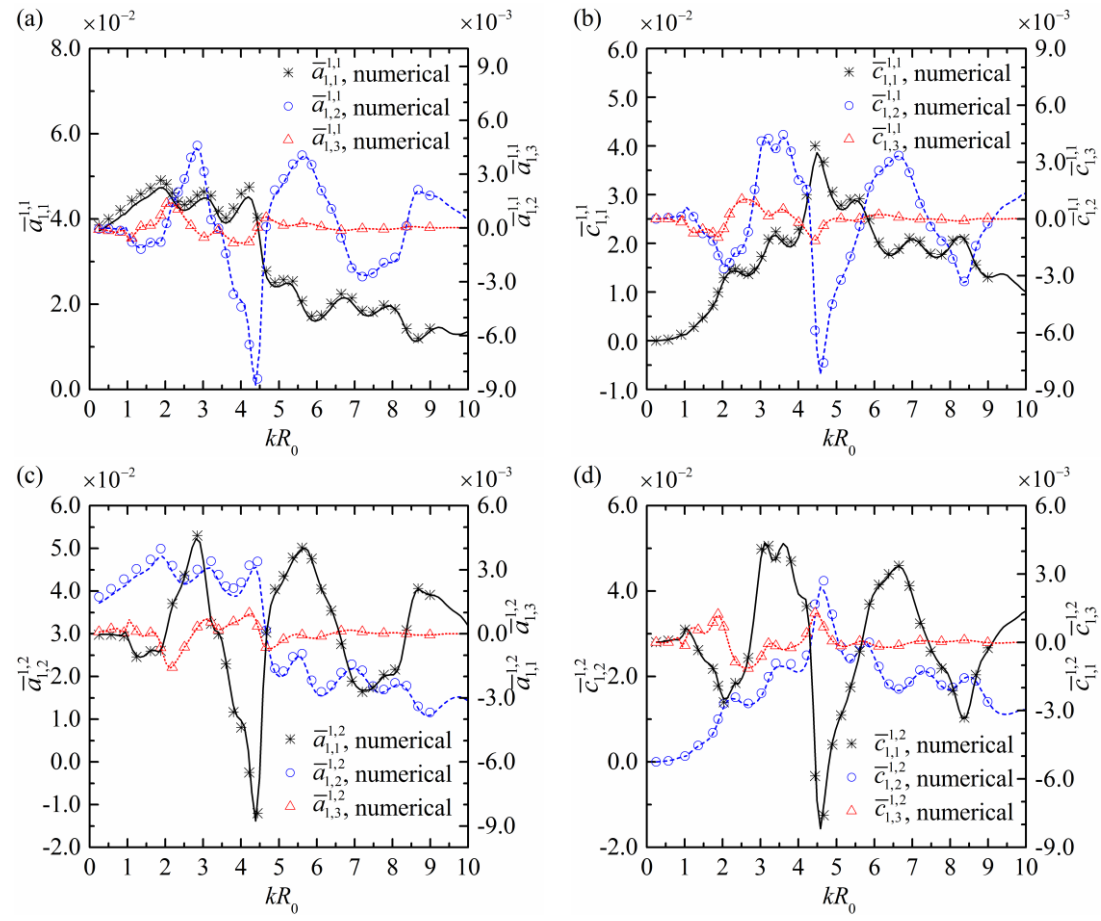

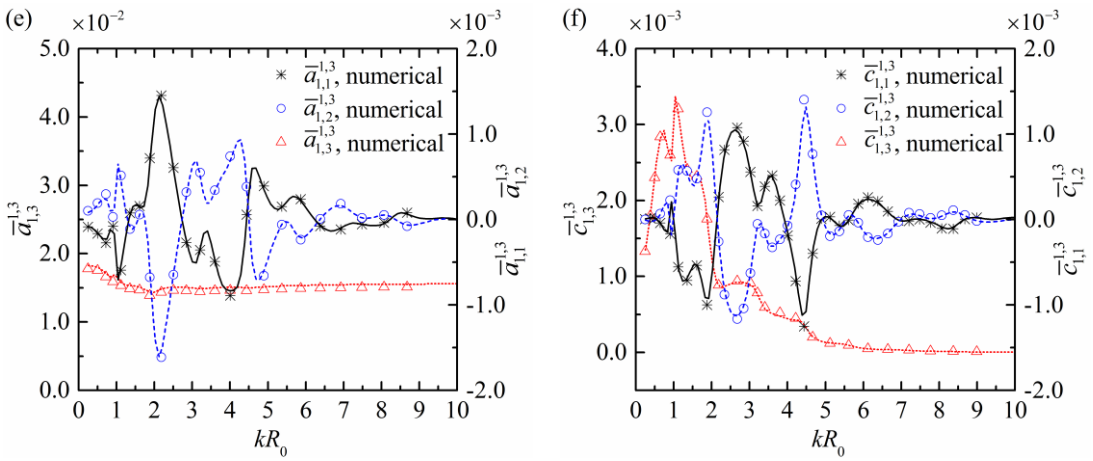

Fig. 12. Hydrodynamic coefficients of Float 1 due to its oscillation. a) $\bar{a}_{1,i}^{1,1}$; b) $\bar{c}_{1,i}^{1,1}$; c) $\bar{a}_{1,i}^{1,2}$; d) $\bar{c}_{1,i}^{1,2}$; e) $\bar{a}_{1,i}^{1,3}$; f) $\bar{c}_{1,i}^{1,3}$. solid line, dash line and dot line: theoretical results.

Hydrodynamic coefficients of one float due to the oscillation of another float reflect the hydrodynamic interaction between these floats. Figure 13 shows these coefficients due to the hydrodynamic interaction between Float 1 and Float 3. The present theoretical method and the numerical method give the same results. Additionally, the relations $\bar{a}_{n,i}^{n',i'} = \bar{a}_{n',i'}^{n,i}$ and $\bar{c}_{n,i}^{n',i'} = \bar{c}_{n',i'}^{n,i}$, so-called reciprocity relations (Falnes, 2002), are also satisfied very well as plotted in both Fig.12 and Fig.13.

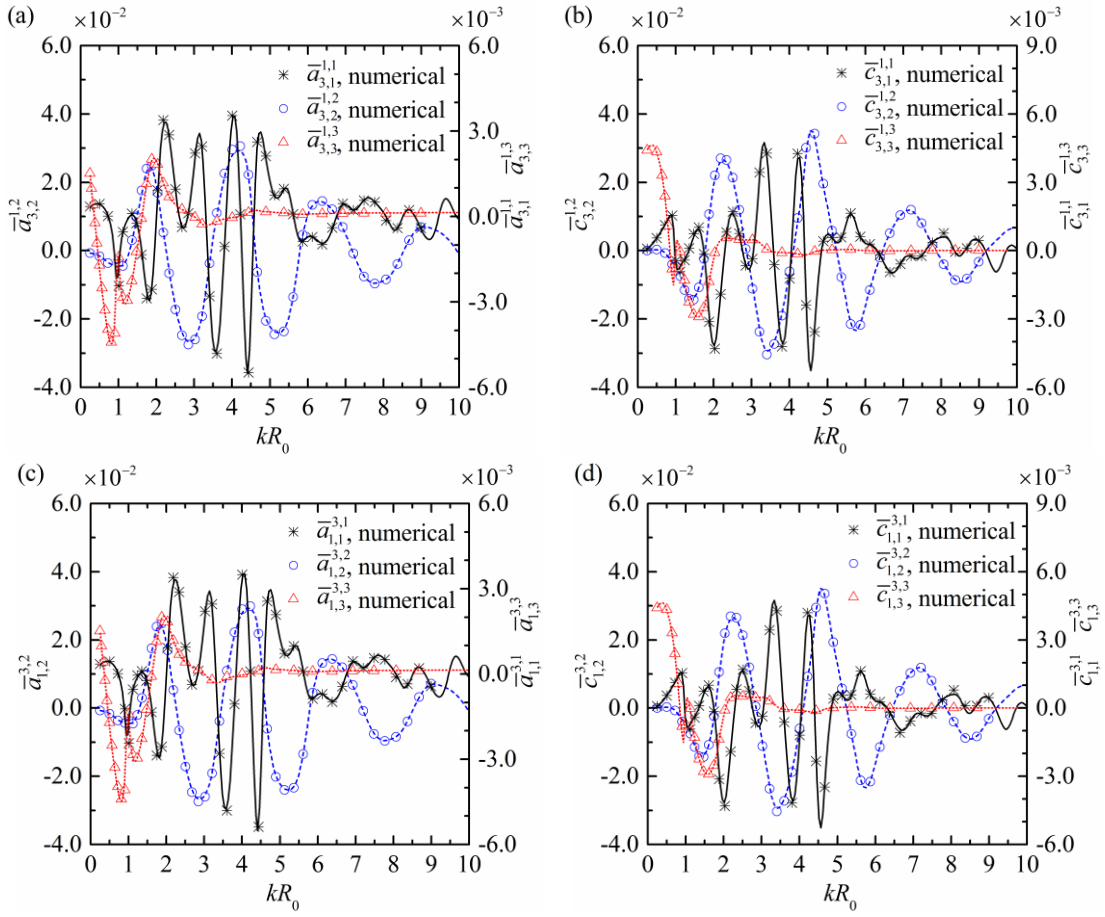

Fig. 13. Hydrodynamic coefficients due to hydrodynamic interaction between Float 1 and Float 3. a) $\bar{a}_{3,i}^{1,i}$; b) $\bar{c}_{3,i}^{1,i}$; c) $\bar{a}_{1,i}^{3,i}$; d) $\bar{c}_{1,i}^{3,i}$. dash line, dot line and solid line: theoretical results.

Figure 14 shows the hydrodynamic coefficients induced by the hydrodynamic interaction between the OWC and Float 1. Both direct method and the expressions based on Haskind relation are employed to calculate $\bar{a}_{n,i}^{(0)}$ and $\bar{a}_{(0)}^{n,i}$, giving the same results as plotted in Figs. 14a and 14c for $\bar{a}_{1,j}^{(0)}$ and $\bar{a}_{(0)}^{1,j}$, respectively. The corresponding $\bar{c}_{1,j}^{(0)}$ and $\bar{c}_{(0)}^{1,j}$ are illustrated in Figs. 14b and 14d. In common with the results of $F_e^{(0)}$ and $F_e^{n,j}$ as shown in Figs. 7, 8 and 9, sharp changes in $\bar{a}_{1,j}^{(0)}$, $\bar{a}_{(0)}^{1,j}$, $\bar{c}_{1,j}^{(0)}$ and $\bar{c}_{(0)}^{1,j}$ also occur around kR_0=1.0. While different from the reciprocity relations of the coefficients due to the hydrodynamic coupling between floats, the coefficients taking account of hydrodynamic interaction between the OWC and floats should satisfy $\bar{a}_{n,i}^{(0)} = -\bar{a}_{(0)}^{n,i}$ and $\bar{c}_{n,i}^{(0)} = -\bar{c}_{(0)}^{n,i}$ (Falnes, 2002), which can also be observed from Fig. 14.

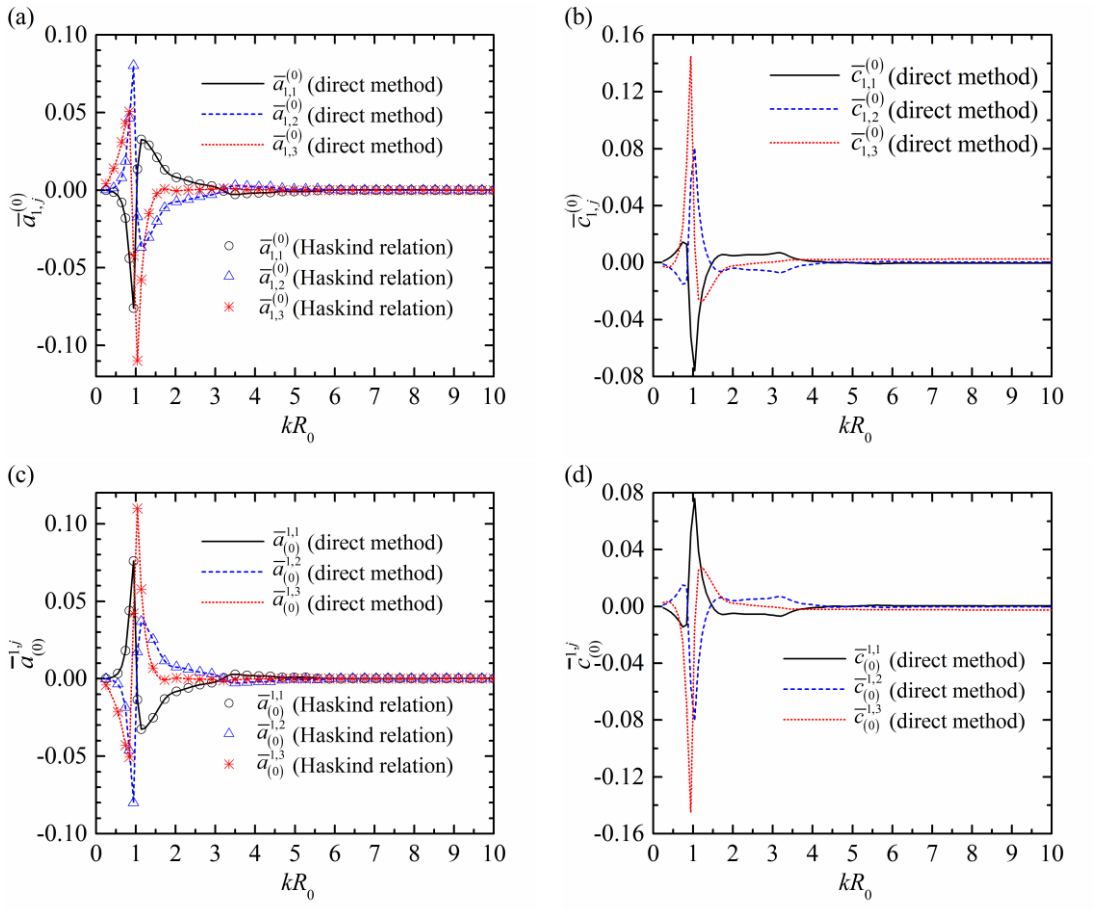

Fig. 14. Hydrodynamic coefficients due to hydrodynamic interaction between the OWC and Float 1. a) $\bar{a}_{1,j}^{(0)}$; b) $\bar{c}_{1,j}^{(0)}$; c) $\bar{a}_{(0)}^{1,j}$; d) $\bar{c}_{(0)}^{1,j}$.

5.2 Comparison between the hybrid WEC and the isolated OWC and hinged floats

In this section, wave extraction of the hybrid WEC is calculated based on the coefficients

obtained from the validated theoretical hydrodynamic model. To recognize the difference in the maximum power capture factor among the hybrid WEC composed of a OWC and several hinged floats, its corresponding OWC and hinged floats which run in isolation, respectively, a comparison between them is carried out. The OWC and these hinged floats which run in isolation are hereinafter called the isolated OWC and hinged floats, respectively. In subsequent computations, wave power extraction by the hybrid WEC consisting of an OWC and four floats (N=4) hinged around is investigated. There are many geometric parameters affecting power absorption of the hybrid WEC. To reduce the number of these parameters, here, it is assumed that the following relations among these parameters are satisfied, $R_0^2 d_0 = 3h^3/320$, R_i=0.8R_0, $R_j^2 d_j = h^3/2000$, D_j=2R_j, h_j=2d_j. Thus the hybrid WEC scales in terms of non-dimensional parameters can be determined once d_0/h and d_1/h are known. The incident waves are considered with propagation direction in x-axis direction as given in Fig.1. Figure 15 gives variation of the maximum power capture factors of the isolated OWC and the hinged floats, respectively, with d_0/h and d_1/h for wave condition kh=3.2. As d_1/h has no effect on power absorption of the isolated OWC, its maximum power capture factor ($\tilde{\eta}_{\max}$) is plotted as a curve (as shown in Fig.15a), rather than a contour as given in Fig.15b for the hinged floats.

It can be seen from Fig.15a that, as d_0/h increases from 0.05, $\tilde{\eta}_{\max}$ first decreases from 0.12 and leads to the valley value of 0.086 at d_0/h=0.13. As d_0/h further increases, $\tilde{\eta}_{\max}$ rises and then decreases after reaching the peak value of 0.158 which occurs at d_0/h=0.22. As studied by Falnes (2002), the maximum power capture factor of the axisymmetric OWC is 1/(2π) when both "optimum phase condition" and "optimum amplitude condition" are satisfied simultaneously, in another words, PTO damping and PTO added mass are instantaneously optimized. The peak value of $\tilde{\eta}_{\max}$, as plotted in Fig. 15a, satisfies 0.158≈1/(2π), meaning that resonance happens for the isolated OWC with d_0/h=0.22 at kh=3.2.

The contour of the maximum power capture factor ($\hat{\eta}_{\max}$) of the isolated hinged floats, as given in Fig.15b, shows that, for kh=3.2, $\hat{\eta}_{\max}$ is more sensitive to d_1/h than d_0/h. For any specified d_0/h, a peak of $\hat{\eta}_{\max}$ occurs when d_1/h is around 0.08. When d_1/h=0.01, a larger d_0/h plays a positive role in improving power absorption. While for d_1/h=0.08, on the contrary, small value of d_0/h, i.e. large spacing distance between the legs as shown in Fig.5, is welcome in maximizing power exploitation. The peak value of $\hat{\eta}_{\max}$ is 0.52 with d_0/h=0.05 and d_1/h=0.078.

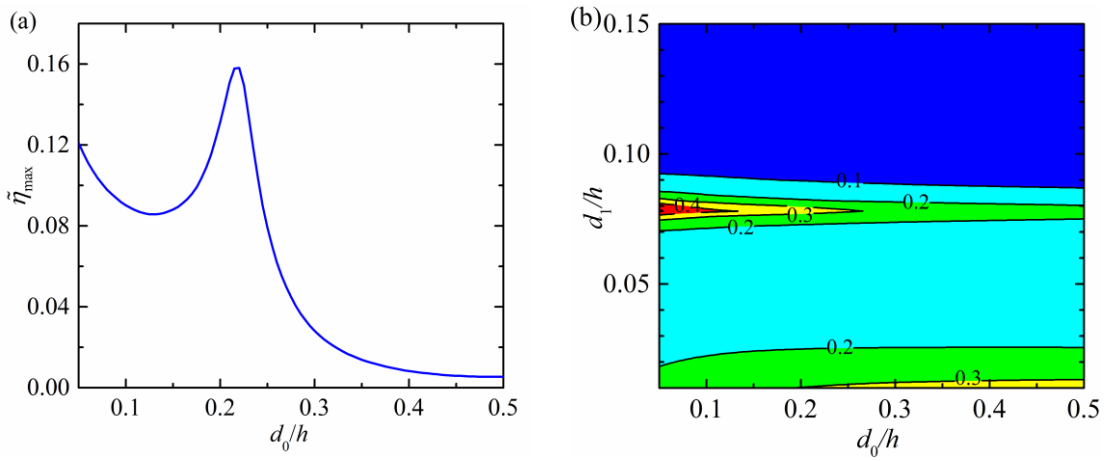

Fig. 15. Maximum power capture factor ($\tilde{\eta}_{max}$ and $\hat{\eta}_{max}$) of the isolated OWC and the isolated hinged floats for $R_0^2 d_0 = 3h^3/320$, R_i=0.8R_0, $R_j^2 d_j = h^3/2000$, D_j=2R_j, h_j=2d_j and kh=3.2: (a) variation of $\tilde{\eta}_{max}$ with d_0/h; (b) variation of $\hat{\eta}_{max}$ with d_0/h and d_1/h.

To demonstrate the difference in the maximum power capture factor between the hybrid WEC and the isolated OWC and hinged floats, and to understand whether the OWC and hinged floats in the hybrid WEC interact beneficially or counteract each other in terms of q-factor, a wide range of d_0/h and d_1/h are examined. For the hybrid WEC, i.e. combining the isolated OWC and the isolated hinged floats together and considering the hydrodynamic interaction between them, the maximum power capture factor (η_{max}) and q-factor for kh=3.2 are plotted in Fig.16. Thanks to the hydrodynamic coupling, the peak value of the maximum power capture factor of the hybrid WEC can be 0.63 when d_0/h=0.05 and d_1/h=0.078, obviously larger than those for the isolated OWC (0.158) and hinged floats (0.52). η_{max}>0.5 can be obtained at the range of d_0/h<0.12 and 0.076<d_1/h<0.080. Different from the distribution of the maximum power capture factor, as shown in Fig.16b, the q-factor larger than 1.5 occurs at the area of d_0/h>0.26 and 0.076<d_1/h<0.080, and the maximum q-factor is 1.79, occuring at d_0/h=0.5 and d_1/h=0.078. For the hybrid WEC with d_0/h>0.25 and d_1/h<0.09, generally q>1.0 can be achieved, which means hydrodynamic coupling plays a constructive effect on power absorption for kh=3.2. While for d_0/h>0.32 and d_1/h>0.12, q-factor could be less than 0.7, resulting in a destructive effect on power extraction. Although the areas corresponding to the largest value of η_{max} and q-factor, respectively, do not coincide, q>0.9 is satisfied in the contour area η_{max} >0.5, where q>1.0 is even valid for some subdomains.

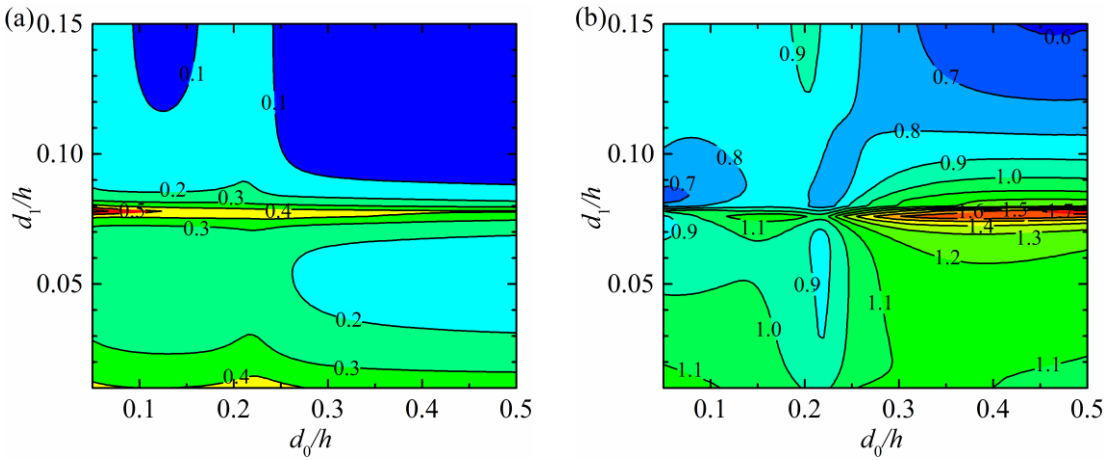

Fig. 16. Maximum power capture factor ($\eta_{\max}$) and q-factor of the hybrid WEC for $R_0^2 d_0 = 3h^3/320$, R_i=0.8R_0, $R_j^2 d_j = h^3/2000$, D_j=2R_j, h_j=2d_j and kh=3.2: (a) contour of $\eta_{\max}$; (b) contour of q-factor.

Apart from the comparison between the isolated OWC and hinged floats and the hybrid WEC carried out for a certain wave condition (kh=3.2), the case with d_0/h=0.15, d_1/h=0.08 is also taken as an example to study the frequency responses of the maximum power absorption, which are plotted in Fig. 17. The peak of the maximum power capture factor of the isolated OWC ($\tilde{\eta}_{\max}$) happens at kh=3.8, reaching 0.158. For the four hinged floats, the peak value of $\hat{\eta}_{\max}$ is 0.378 when kh=3.0. Compared with the isolated OWC and hinged floats, the hybrid WEC holds a wider bandwidth of frequency response with a larger maximum power capture factor, as shown in Fig.17a. The corresponding q-factor response (as plotted in Fig.17b) shows that q>0.9 can be satisfied for all the wave conditions except for 3.1<kh <4.5. What is better, two peaks of q-factor, one is q=1.3 at kh=2.9, the other is q=2.3 at kh=8.9, are obtained. For any wave conditions with kh>4.9, q>1 is achieved, i.e., the hydrodynamic coupling between the OWC and the floats in the hybrid WEC plays a constructive effect on overall power absorption. Therefore, it is believed that the hybrid WEC could perform much better in realistic wave climates in terms of power extraction compared with those for the isolated OWC and hinged floats.

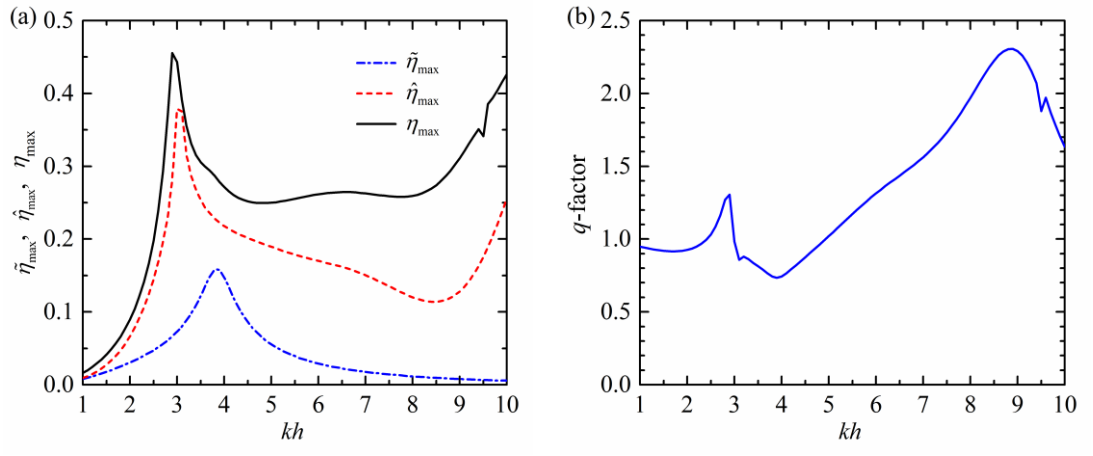

Fig. 17. Frequency response of the maximum power capture factor ($\tilde{\eta}_{max}$, $\hat{\eta}_{max}$ and η_{max}) of the isolated OWC, the isolated hinged floats, the hybrid WEC and the *q*-factor for $R_0^2 d_0 = 3h^3/320$, R_i=0.8R_0, $R_j^2 d_j = h^3/2000$, D_j=2R_j, h_j=2d_j, d_0/h=0.15, d_1/h=0.08. (a) $\tilde{\eta}_{max}$, $\hat{\eta}_{max}$ and η_{max}; (b) *q*-factor .

5.3 Spacing distance between the OWC and the floats

To investigate the effect of the spacing distance between the OWC and the floats on power absorption, four cases of the hybrid WEC with D_j=2R_j, 3R_j , 4R_j and 5R_j, respectively, are studied. Results of the frequency response of η_{max}, together with the power capture factor of the OWC and each float of the hybrid WEC are plotted in Fig. 18. Since the incident waves propagate along *x*-axis and *y*=0 is a plane of symmetry of the hybrid WEC, power capture factors of Float 2 and Float 4 denoted as $\eta_{max}^{(2)}$ and $\eta_{max}^{(4)}$, respectively, as shown in Fig.18, are all the same for any specified wave conditions. It can be seen from Fig. 18 that the larger D_j is, the bigger *kh* is which corresponds to the peak value of η_{max}. The peak value of η_{max} and the corresponding *kh* for D_j=2R_j, 3R_j , 4R_j and 5R_j are (0.455, 2.9), (0.658, 4.4), (0.516, 5.3) and (0.556, 7.2), respectively. The peak of the $\eta_{max}^{(3)}$–*kh* curve happens at the same *kh* when the peak of η_{max} occurs. In long waves (*kh*<2.0), the power absorbed by the OWC is far larger than the power extracted by any of the floats. While in short waves (*kh*>8.0), the power is mainly captured by the floats of the hybrid WEC rather than the OWC and the power absorbed by the OWC is much smaller than the power absorbed by the float which extracted the least power in the floats.

For D_j=2R_j and D_j=3R_j, as shown in Figs. 18a and 18b, it should be noted that there are almost no power being absorbed by the OWC and most of the power are captured by the floats when η_{max} reaches the peaks. Meanwhile, the power extracted by Float 3, the windward one, is nearly always larger than that of any other three floats, which might be attributed to the constructive effect of the wave reflected by the OWC for these specified dimension parameters. While for D_j=4R_j and D_j=5R_j, as shown in Figs. 18c and 18d, Floats 2 and 4, i.e., the side floats, turn to capture more power than any other three floats for a wide range of wave frequencies.

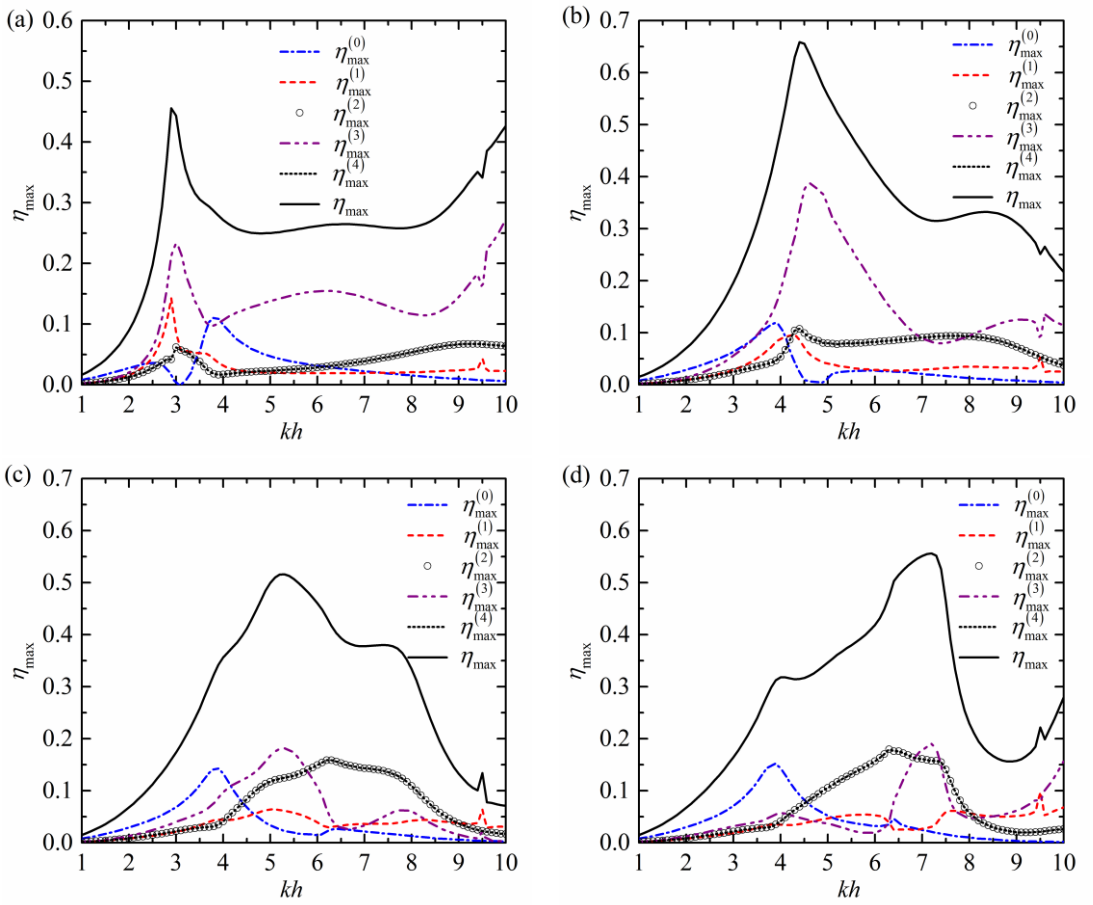

Fig. 18. Frequency response of the maximum power capture factor (η_{max}) of the hybrid WEC with different spacing distance between the OWC and the floats for $R_0^2 d_0 = 3h^3/320$, R_i=0.8R_0, $R_j^2 d_j = h^3/2000$, h_j=2d_j, d_0/h=0.15, d_1/h=0.08. (a) D_j=2R_j; (b) D_j=3R_j;.(c) D_j=4R_j; (d) D_j=5R_j.

6 Conclusions

A novel hybrid WEC consisting of a floating OWC moored at the sea bed and several floats hinged around is presented. To study hydrodynamic performance of the hybrid WEC, a theoretical hydrodynamic model is developed to solve the wave diffraction and radiation problems from a cylindrical OWC and several truncated floats oscillating independently in surge, sway, heave, roll, pitch and yaw modes based on the linear wave theory. Wave excitation volume flux/forces and hydrodynamic coefficients are evaluated by using the diffracted and near field radiated potentials, respectively. Moreover, some hydrodynamic coefficients are also obtained with other two approaches, one is in terms of the Far-Field Coefficients and the other is by wave excitation volume flux/forces.

To testify the validity of this theoretical hydrodynamic model, numerical computations with the use of a boundary element method commercial code are also carried out, and the theoretical results by applying three different approaches and the numerical ones are compared with each other. The theoretical results are found in good agreement with ones obtained by using different approaches.

The validated theoretical hydrodynamic model is finally used to learn the power extraction by a hybrid WEC consisting of an OWC and four floats hinged around. The results reveal that:

1) Due to the hydrodynamic coupling, the peak value of the maximum power capture factor of the hybrid WEC can be 0.63 for $R_0^2 d_0 = 3h^3/320$, R_i=0.8R_0, $R_j^2 d_j = h^3/2000$, D_j=2R_j, h_j=2d_j and kh=3.2, obviously larger than those for the isolated OWC (0.158) and the isolated hinged floats (0.52).

2) Compared with the isolated OWC and hinged floats, the hybrid WEC holds a wider bandwidth of frequency response with a higher maximum power capture factor.

3) In long waves, the power absorbed by the OWC is far larger than the power extracted by any of the floats. While in short waves, the power is mainly captured by the floats in the hybrid WEC rather than the OWC.

4) As spacing distance between the OWC and the floats increases from 2R_j to 5R_j, the peak of the maximum power capture factor ($\eta_{\max}$) of the hybrid WEC occurs at a higher wave frequency.

Apart from improving power capture ability of the isolated OWC and hinged floats by combining them together, apparently the hybrid WEC has an advantage in reducing construction costs.

The present paper only presents a fundamental study of the hybrid WEC in regular waves. Effect of the multiple parameters, such as wave incident direction and float number, and the performance of the hybrid WEC in realistic wave climates deserve further investigation in the near future. The study carried out in this paper is based on the linearised hydrodynamic theory for an ideal irrotational fluid. Since the viscous effect is not taken into consideration, wave power absorption may be overestimated by using the potential flow theory. The viscous effect on the hybrid WEC might be investigated by using physical experiments in the future.

Acknowledgements

The research was supported by the National Natural Science Foundation of China (51679124, 51479092), China Postdoctoral Science Foundation (Grant No. 2016M601041, 2017T100085) and Tsinghua National Laboratory for Information Science and Technology.

Appendix A. Derivation process of the formulas and calculation for the unknown coefficients of diffracted potentials

Substitute the diffracted spatial potentials in Eqs. (12)~(22) and wave incident potential given in Eq.(2b) into Eqs. (23)~(24), then after multiplying both sides by $\mathrm{e}^{-\mathrm{i}\tau\theta_j}\cos\left[\beta_{j,\varsigma}\left(z+h\right)\right]$ and integrating for $\theta_j \in [0, 2\pi]$ and $z \in \left[-h, -d_j\right]$, we get:

$$\begin{aligned} &-A_{\tau,\zeta}^{\mathrm{D},j} - \delta_{n,0} C_{\tau,\zeta}^{\mathrm{D},j} + 2\sum_{l=0}^{\infty} B_{\tau,l}^{\mathrm{D},j} L_{l,\zeta}^{(j)} + 2\sum_{\substack{j'=0 \\ j'\neq j}}^{N} \sum_{m=-\infty}^{\infty} \sum_{l=0}^{\infty} B_{m,l}^{\mathrm{D},j'} T_{m,\tau,l}^{n,j'} L_{l,\zeta}^{(j)} \\ &= \frac{2\mathrm{i}gA}{\omega} \mathrm{i}^{\tau} J_{\tau}\left(k_0 R_n\right) L_{0,\zeta}^{(j)} \mathrm{e}^{\mathrm{i}k_0\left(x_j\cos\beta + y_j\sin\beta\right)} \mathrm{e}^{-\mathrm{i}\tau\beta} \end{aligned}, \quad (A.1)$$

$$-a_{\tau,\zeta} A_{\tau,\zeta}^{\mathrm{D},0} - b_{\tau,\zeta} C_{\tau,\zeta}^{\mathrm{D},0} + 2\sum_{l=0}^{\infty} D_{\tau,l}^{\mathrm{D},N+1} L_{l,\zeta}^{(0)} = \frac{2\mathrm{i}gA}{\omega} \mathrm{i}^{\tau} J_{\tau}\left(k_0 R_{\mathrm{i}}\right) L_{0,\zeta}^{(0)} \mathrm{e}^{\mathrm{i}k_0\left(x_0\cos\beta + y_0\sin\beta\right)} \mathrm{e}^{-\mathrm{i}\tau\beta}, \quad (A.2)$$

where

$$L_{l,\varsigma}^{(j)}=\frac{1}{h-d_j}\int_{-h}^{-d_j}\frac{Z_l\left(z\right)\cos\left[\beta_{j,\varsigma}\left(z+h\right)\right]}{Z_l\left(0\right)}\mathrm{d}z$$

$$=\begin{cases}\dfrac{\left(-1\right)^{\varsigma}\left(h-d_j\right)k_0\sinh\left[k_0\left(h-d_j\right)\right]}{\left[\left(h-d_j\right)^2k_0^2+\varsigma^2\pi^2\right]\cosh\left(k_0h\right)}, & l=0;\varsigma=0,1,2\cdots\\ \dfrac{\left(-1\right)^{\varsigma}\left(h-d_j\right)k_l\sin\left[k_l\left(h-d_j\right)\right]}{\left[\left(h-d_j\right)^2k_l^2-\varsigma^2\pi^2\right]\cos\left(k_lh\right)}, & l=1,2,3\cdots;\varsigma=0,1,2\cdots\end{cases}, \tag{A.3}$$

$$T_{m,\tau,l}^{j,j'}=\begin{cases}\dfrac{\left(-1\right)^{\tau}H_{m-\tau}\left(k_0R_{jj'}\right)J_{\tau}\left(k_0R_j\right)\mathrm{e}^{\mathrm{i}\left(m\alpha_{j'j}-\tau\alpha_{jj'}\right)}}{H_m\left(k_0R_{j'}\right)}, & l=0\\ \dfrac{K_{m-\tau}\left(k_lR_{jj'}\right)I_{\tau}\left(k_lR_j\right)\mathrm{e}^{\mathrm{i}\left(m\alpha_{j'j}-\tau\alpha_{jj'}\right)}}{K_m\left(k_lR_{j'}\right)}, & l=1,2,3\cdots\end{cases}, \tag{A.4}$$

$$a_{\tau,\zeta}=\begin{cases}\left(\dfrac{R_{\mathrm{i}}}{R_0}\right)^{|\tau|}, & \zeta=0\\ \dfrac{I_{\tau}\left(\beta_{0,\zeta}R_{\mathrm{i}}\right)}{I_{\tau}\left(\beta_{0,\zeta}R_0\right)}, & \zeta\neq0\end{cases};\quad b_{\tau,\zeta}=\begin{cases}1+\ln\left(\dfrac{R_{\mathrm{i}}}{R_0}\right), & \zeta=0;\tau=0\\ \left(\dfrac{R_{\mathrm{i}}}{R_0}\right)^{-|\tau|}, & \zeta=0;\tau\neq0\\ \dfrac{K_{\tau}\left(\beta_{0,\zeta}R_{\mathrm{i}}\right)}{K_{\tau}\left(\beta_{0,\zeta}R_0\right)}, & \zeta\neq0\end{cases}. \tag{A.5}$$

Similarly, substitute the diffracted spatial potentials in Eqs. (12)~(22) and wave incident potential given in Eq.(2b) into Eqs. (25)~(26), after multiplying both sides by $\mathrm{e}^{-\mathrm{i}\tau\theta_j}Z_{\varsigma}\left(z\right)$ and integrating for $\theta_j\in\left[0,2\pi\right]$ and $z\in\left[-h,0\right]$, we have:

$$-\sum_{l=0}^{\infty}A_{\tau,l}^{\mathrm{D},j}\Lambda_{\tau,l}^{(j)}Z_{\varsigma}\left(0\right)L_{\zeta,l}^{(j)}-\delta_{n,0}\sum_{l=0}^{\infty}C_{\tau,l}^{\mathrm{D},j}X_{\tau,l}^{(j)}Z_{\zeta}\left(0\right)L_{\zeta,l}^{(j)}+B_{\tau,\zeta}^{\mathrm{D},j}\Pi_{\tau,\zeta}^{(j)}+\sum_{\substack{j'=0\\j'\neq j}}^{N}\sum_{m=-\infty}^{\infty}B_{m,\zeta}^{\mathrm{D},j'}T_{m,\tau,\zeta}^{\prime j,j'}$$

$$=\delta_{\zeta,0}\frac{\mathrm{i}^{\tau+1}\mathrm{e}^{\mathrm{i}k_0\left(x_j\cos\beta+y_j\sin\beta\right)}\mathrm{e}^{-\mathrm{i}\tau\beta}gAk_0J_{\tau}'\left(k_0R_j\right)}{\omega Z_0\left(0\right)}, \tag{A.6}$$

$$-\sum_{l=0}^{\infty}a_{\tau,l}'A_{\tau,l}^{\mathrm{D},0}\Lambda_{\tau,l}^{(0)}Z_{\zeta}\left(0\right)L_{\zeta,l}^{(0)}-\sum_{l=0}^{\infty}b_{\tau,l}'C_{\tau,l}^{\mathrm{D},0}X_{\tau,l}^{(0)}Z_{\zeta}\left(0\right)L_{\zeta,l}^{(0)}+D_{\tau,\zeta}^{\mathrm{D},N+1}\Pi_{\tau,\zeta}^{\prime(0)}$$

$$=\delta_{\zeta,0}\frac{\mathrm{i}^{\tau+1}\mathrm{e}^{\mathrm{i}k_0\left(x_0\cos\beta+y_0\sin\beta\right)}\mathrm{e}^{-\mathrm{i}\tau\beta}gAk_0J_{\tau}'\left(k_0R_{\mathrm{i}}\right)}{\omega Z_0\left(0\right)}, \tag{A.7}$$

where

$$\Lambda_{\tau,l}^{(j)}=\begin{cases}\dfrac{|\tau|\left(h-d_j\right)}{2R_jh}, & l=0\\ \dfrac{\beta_{j,l}I_\tau'\left(\beta_{j,l}R_j\right)\left(h-d_j\right)}{I_\tau\left(\beta_{j,l}R_j\right)h}, & l=1,2,3\cdots\end{cases}, \tag{A.8}$$

$$X_{\tau,l}^{(0)}=\begin{cases}\dfrac{h-d_0}{2R_0h}, & l=0,\tau=0\\ \dfrac{-|\tau|\left(h-d_0\right)}{2R_0h}, & l=0,\tau\neq 0\\ \dfrac{\beta_{0,l}K_\tau'\left(\beta_{0,l}R_0\right)\left(h-d_0\right)}{K_\tau\left(\beta_{0,l}R_0\right)h}, & l=1,2,3\cdots\end{cases}, \tag{A.9}$$

$$\Pi_{\tau,l}^{(j)}=\begin{cases}\dfrac{k_0H_\tau'\left(k_0R_j\right)}{H_\tau\left(k_0R_j\right)Z_0\left(0\right)}, & l=0\\ \dfrac{k_lK_\tau'\left(k_lR_j\right)}{K_\tau\left(k_lR_j\right)Z_l\left(0\right)}, & l=1,2,3\cdots\end{cases};\quad \Pi_{\tau,l}'^{(0)}=\begin{cases}\dfrac{k_0J_\tau'\left(k_0R_i\right)}{J_\tau\left(k_0R_i\right)Z_0\left(0\right)}, & l=0\\ \dfrac{k_lI_\tau'\left(k_lR_i\right)}{I_\tau\left(k_lR_i\right)Z_l\left(0\right)}, & l=1,2,3\cdots\end{cases}, \tag{A.10}$$

$$T'^{j,j'}_{m,\tau,l}=\begin{cases}\dfrac{(-1)^\tau k_0J_\tau'\left(k_0R_j\right)H_{m-\tau}\left(k_0R_{jj'}\right)\mathrm{e}^{\mathrm{i}\left(m\alpha_{j'j}-\tau\alpha_{jj'}\right)}}{H_m\left(k_0R_{j'}\right)Z_0\left(0\right)}, & l=0\\ \dfrac{k_lI_\tau'\left(k_lR_j\right)K_{m-\tau}\left(k_lR_{jj'}\right)\mathrm{e}^{\mathrm{i}\left(m\alpha_{j'j}-\tau\alpha_{jj'}\right)}}{K_m\left(k_lR_{j'}\right)Z_l\left(0\right)}, & l=1,2,3\cdots\end{cases}, \tag{A.11}$$

$$a'_{\tau,l}=\begin{cases}1, & l=0,\tau=0\\ \left(\dfrac{R_i}{R_0}\right)^{|\tau|-1}, & l=0,\tau\neq 0\\ \dfrac{I_\tau'\left(\beta_{0,l}R_i\right)}{I_\tau'\left(\beta_{0,l}R_0\right)}, & l\neq 0\end{cases};\quad b'_{\tau,l}=\begin{cases}\dfrac{R_0}{R_i}, & l=0;\tau=0\\ \left(\dfrac{R_i}{R_0}\right)^{-|\tau|-1}, & l=0;\tau\neq 0\\ \dfrac{K_\tau'\left(\beta_{0,l}R_i\right)}{K_\tau'\left(\beta_{0,l}R_0\right)}, & l\neq 0\end{cases}, \tag{A.12}$$

$2(N+2)(2M+1)(L_0+1)$ complex linear equations with an equal number of unknown coefficients can be obtained from Eqs.(A1), (A2), (A6) and (A7) after truncation of $\mathrm{e}^{\mathrm{i}m\theta}$ (m=-M, …, 0, …, M), Z_l(z) and $\cos[\beta_{j,l}(z+h)]$ (l=0, 1, 2, … L_0) functions. Therefore, the unknown coefficients can be easily calculated by solving the complex $2(N+2)(2M+1)(L_0+1)$ order linear matrix equation.

For the radiated spatial potentials due to float oscillation and those due to air pressure oscillation inside the OWC, similar expressions can also be derived. Note Eqs.(A1), (A2), (A6) and those for radiated spatial potentials share the same $2(N+2)(2M+1)(L_0+1)$ order linear complex coefficient matrix, hence wave diffraction and wave radiation problems can be solved simultaneously.

References

Abramowitz, M., Stegun, I.A., 1964. Handbook of Mathematical Functions. Government Printing Office, Washington, DC.

Babarit, A., 2013. On the park effect in arrays of oscillating wave energy converters. Renewable Energy. 58, 68-78.

Babarit, A., Hals, J., Muliawan, M.J., et al., 2012. Numerical benchmarking study of a selection of wave energy converters. Renewable Energy. 41, 44-63.

Borgarino, B., Babarit, A., Ferrant, P., 2012. Impact of wave interactions effects on energy absorption in large arrays of wave energy converters. Ocean Engineering. 41, 79-88.

Clément, A., McCullen, P., Falcão, A., 2002. Wave energy in Europe: current status and perspectives. Renewable and Sustainable Energy Reviews. 6, 405-431.

Cruz, J.E., Ocean Wave Energy: Current Status and Future Perspectives. 2008: Springer.

Cruz, J.M.B.P., Salter, S.H., 2006. Numerical and experimental modelling of a modified version of the Edinburgh Duck wave energy device. Proceedings of the Institution of Mechanical Engineers Part M: Journal of Engineering for the Maritime Environment. 220(3), 129-147.

Davies, P.A., 2005. Wave-powered desalination: resource assessment and review of technology. Desalination. 186, 97-109.

Drew, B., Plummer, A.R., Sahinkaya, M.M., 2009. A review of wave energy converter technology. Proceedings of the Institution of Mechanical Engineers Part A Journal of Power and Energy. 223(8): 887-902.

Evans, D.V., 1982.Wave-power absorption by systems of oscillating surface pressure distributions. Journal of Fluid Mechanics. 114, 481-499.

Evans, D.V., Porter, R., 1995. Hydrodynamics characteristics of an oscillating water column device. Applied Ocean Research. 17, 155-164.

Evans, D.V., Porter, R., 1997. Efficient calculation of hydrodynamic properties of OWC-type devices. Journal of Offshore Mechanics and Arctic Engineering. 119(4), 210-218.

Falcão, A.F.O., 2010. Wave energy utilization: A review of the technologies. Renewable and Sustainable Energy Reviews. 14, 899-918.

Falcão, A.F.O., Henriques, J.C.C., 2016. Oscillating-water-column wave energy converters and air turbines: A review. Renewable Energy. 85, 1391-1424.

Falnes, J., 2002. Ocean Waves and Oscillating Systems. Cambridge University Press.

Falnes, J., 2007. A review of wave-energy extraction. Marine Structures. 20, 185-201.

Göteman, M., 2017. Wave energy parks with point-absorbers of different dimensions. Journal of Fluids and Structures. 74, 142-157.

He, F., Huang, Z., 2014. Hydrodynamic performance of pile-supported OWC-type structures as breakwaters: An experimental study. Ocean Engineering. 88, 618-626.

He, F., Huang, Z., 2017. Characteristics of orifices for modeling nonlinear power take-off in wave-flume tests of oscillating water column device. Journal of Zhejiang University-Science A: Applied Physics and Engineering. 18(5), 329-345.

Heath, T.V., 2012. A review of oscillating water columns. Philosophical Transactions of the Royal Society A. 370, 235-245.

Konispoliatis, D.N., Mavrakos, S.A., 2016. Hydrodynamic analysis of an array of interacting free-floating oscillating water column (OWC's) devices. Ocean Engineering. 111, 179-197.

Lehmann, M., Karimpour, F., Goudey, C.A., et al., 2017. Ocean wave energy in the United States: Current status and future perspectives. Renewable and Sustainable Energy Reviews. 74, 1300-1313.

López, I, Andreu, J., Ceballos, S., et al., 2013. Review of wave energy technologies and the necessary

power-equipment. Renewable and Sustainable Energy Reviews. 27, 413-434.

Lovas, S., Mei, C.C., Liu, Y., 2010. Oscillating water column at a coastal corner for wave power extraction. Applied Ocean Research. 32, 267-283.

Martins-rivas, H., Mei, C.C., 2009a. Wave power extraction from an oscillating water column at the tip of a breakwater. Journal of Fluid Mechanics.626, 395-414.

Martins-rivas, H., Mei, C.C., 2009b. Wave power extraction from an oscillating water column along a straight coast. Ocean Engineering. 36, 426-433.

Mavrakos, S.A., Konispoliatis, D.N., 2012. Hydrodynamics of a free floating vertical axisymmetric oscillating water column device. Journal of Applied Mathematics. Article No. 142850. DOI: 10.1155/2012/142850.

Nambiar, A.J., Forehand, D.I.M., Kramer, M.M., et al., 2015. Effects of hydrodynamic interactions and control within a point absorber array on electrical output. International Journal of Marine Energy. 9, 20-40.

Penalba, M., Kelly, T., Ringwood, J., 2017a. Using NEMOH for modelling wave energy converters: A comparative study with WAMIT. Proceedings of 12th European Wave and Tidal Energy Conference. Cork, Ireland.

Penalba, M., Touzón, I., Lopez-Mendia, J., et al., 2017b. A numerical study on the hydrodynamic impact of device slenderness and array size in wave energy farms in realistic wave climates. Ocean Engineering. 142, 224-232.

Ricci, P., Saulnier, J.B., Falcão, A.F.O., 2007. Point-absorber arrays: a configuration study of the Portuguese west-coast. Proceedings of the 7th European Wave and Tidal Energy Conference, Porto, Portugal, September 11-13.

Salter, S., 1974. Wave power. Nature 249, 720-724.

Serman, D.D. and C.C. Mei, 1980. Note on Salter's energy absorber in random waves. Ocean Engineering **7**(4), 477-490.

Sheng, W, Alcorn, R., Lewis, A., 2014. Assessment of primary energy conversions of oscillating water columns. I. Hydrodynamic analysis. Journal of Renewable and Sustainable Energy. 6,053113(2014); DOI: 10.1063/1.4896850.

Sheng, W., Lewis, A., 2017. Power takeoff optimization to maximize wave energy conversions for oscillating water column devices. IEEE Journal of Oceanic Engineering. DOI: 10.1109/JOE.2016.2644144.

Siddorn, P., Eatock Taylor, R., 2008. Diffraction and independent radiation by an array of floating cylinders. Ocean Eng. 35, 1289-1303.

Thorpe, T. W. 1999. A brief review of wave energy, Technical report no. R120, Energy Technology Support Unit (ETSU), A report produced for the UK Department of Trade and Industry, 1999.

Wu, J., Yao, Y., Zhou, L., et al., 2017. Performance analysis of solo Duck wave energy converter arrays under motion constraints. Energy. 139(15), 155-169.

Yang, J., Zhang, D., Chen, Y., et al., 2017. Design, optimization and numerical modelling of a noval floating pendulum wave energy converter with tide adaptation. China Ocean Engineering. 31(5), 578-588.

Zheng, S., Zhang Y., 2015. Wave diffraction from a truncated cylinder in front of a vertical wall. Ocean Engineering. 104, 329-343.

Zheng, S., Zhang Y., 2016. Wave radiation from a truncated cylinder in front of a vertical wall. Ocean Engineering. 111, 602-614.